First-principles statistical mechanics of structural stability of intermetallic compounds

Z. W. Lu, S.-H. Wei, and Alex Zunger
Solar Energy Research Institute, Golden, Colorado 80401

S. Frota-Pessoa and L. G. Ferreira
Instituto de Física, Universidade de São Paulo, Postal 20516, 01498 São Paulo, Brazil
(Received 4 October 1990)

While as elemental solids, Al, Ni, Cu, Rh, Pd, Pt, and Au crystallize in the face-centered-cubic (fcc) structure, at low temperatures, their 50%-50% compounds exhibit a range of structural symmetries: CuAu has the fcc-based $L1_0$ structure, CuPt has the rhombohedral $L1_1$ structure, and CuPd and AlNi have the body-centered-cubic $B2$ structure, while CuRh does not exist (it phase separates into Cu and Rh). Phenomenological approaches attempt to rationalize this type of structural selectivity in terms of classical constructs such as atomic sizes, electronegativities, and electron/atom ratios. More recently, attempts have been made at explaining this type of selectivity in terms of the (quantum-mechanical) electronic structure, e.g., by contrasting the self-consistently calculated total electron+ion energy of various ordered structures. Such calculations, however, normally select but a small, $O(10)$ subset of "intuitive structures" out of the 2^N possible configurations of two types of atoms on a fixed lattice with N sites, searching for the lowest energy. We use instead first-principles calculations of the total energies of $O(10)$ structures to define a multispin Ising Hamiltonian, whose ground-state structures can be systematically searched by using methods of lattice theories. Extending our previous work on semiconductor alloys [S.-H. Wei, L. G. Ferreira, and A. Zunger, Phys. Rev. B **41**, 8240 (1990)], this is illustrated here for the intermetallic compounds AlNi, CuRh, CuPd, CuPt, and CuAu, for which the correct ground states are identified out of ~65 000 configurations, through the combined use of the density-functional formalism (to extract Ising-type interaction energies) with a simple configurational-search strategy (to find ground states). This establishes a direct and systematic link between the electronic structure and phase stability.

I. INTRODUCTION

Numerous binary $A_{1-x}B_x$ alloys of elemental constituents A and B form at higher temperatures homogeneously disordered solid solutions. As the temperature is lowered, the existence of finite interactions between atoms A and B on the lattice leads either to phase separa- tion or to the formation of various types of long-range or- dered compounds. For example, while as elemental solids, Al, Ni, Cu, Rh, Pd, Pt, and Au appear in the face-centered-cubic (fcc) structure,[1] and form at high temperature binary alloys with the same underlying fcc symmetry,[2-7] when these 50%-50% alloys are cooled down, they exhibit[2-7] distinctly different structural sym-

TABLE I. This table collects some empirical and calculated data on the binary compounds studied here, such as lattice mismatch $\Delta a/a = 2|a_A - a_B|/(a_A + a_B)$, formation enthalpies ΔH, the difference between the calculated (Hartree-Fock) s and d orbital energies of the A and B atoms, and the difference $\chi_A - \chi_B$ in their Pauling electronegativities. Such scales have been previously used to assess qualitative trends in structural preferences.

Binary	Low temp. structure[a] $x=\frac{1}{2}$	$\Delta a/a$[b] (%)	ΔH_{expt} (meV/atom)	$\epsilon_s(A)-\epsilon_s(B)$ Hartree-Fock[e] (eV)	$\epsilon_d(A)-\epsilon_d(B)$ Hartree-Fock[e] (eV)	$\chi_A-\chi_B$ Pauling
AlNi	$B2$	13.9	-741[c]	-3.19		-0.3
CuRh	Separated	5.1	>0[d]	-0.89	-3.51	-0.3
CuPt	$L1_1$	8.2	-174.3[d]	-0.78	-3.38	-0.3
CuPd	$B2$	7.3	-142.3[d]	-0.71	-2.25	-0.3
CuAu	$L1_0$	12.0	-90.7[d]	-0.63	-2.16	-0.5

[a]References 3–7.
[b]Reference 1.
[c]Reference 7(b).
[d]Reference 5 at $x=0.4$.
[e]Reference 14.
[f]Reference 8.

metries: CuAu orders in the fcc $L1_0$ structure, CuPd and AlNi order in the body-centered-cubic (bcc) $B2$ structure, CuPt crystallizes in the rhombohedral $L1_1$ structure, while CuRh phase separates (Fig. 1). Such structural
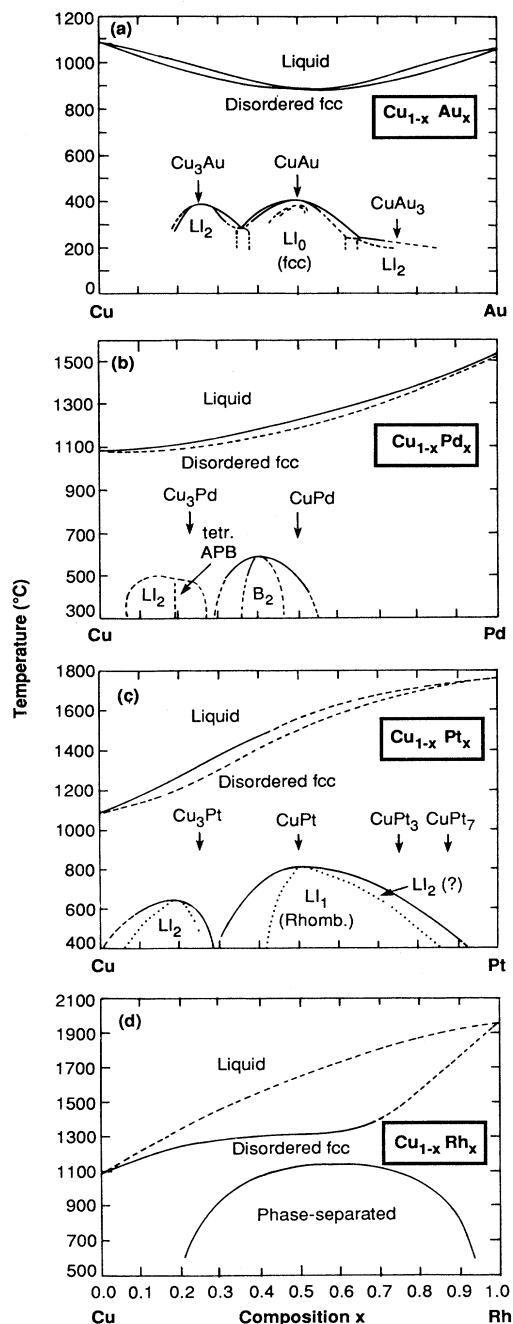

FIG. 1. Experimental (Refs. 3–7) phase diagrams of (a) $Cu_{1-x}Au_x$, (b) $Cu_{1-x}Pd_x$, (c) $Cu_{1-x}Pt_x$, and (d) $Cu_{1-x}Rh_x$. Despite the fact that the pure constituents have the fcc structure and that the solid solutions too have this Bravais lattice, at low temperature these materials show a variety of symmetries for ordered compounds.

preferences in AB compounds have traditionally been discussed in terms of metallurgical and chemical constructs such as the A-B electronegativity difference,[8] size mismatch,[9–11] electron per atom ratios,[9] or differences in A-B orbital radii.[12] Table I summarizes some of these quantities,[13–15] highlighting the fact that (i) this group of compounds exhibits a significant spread in some of these properties, yet, (ii) it is not obvious that the structural preferences are encoded in such simple physical quantities. For example, CuRh and CuPt have similar electronegativity differences as well as s-orbital and d-orbital energy differences, yet they have fundamentally different structural preferences; similar comments pertain to the CuPd and CuAu pair. Also, despite the smaller size mismatch and greater electronegativity difference (both supposed to enhance stability[11]) in Cu-Au relative to Al-Ni, the latter is far stabler than the former (compare their formation enthalpies in Table I).

Understanding of the microscopic origins of this type of structural selectivity has been at the core of structural chemistry, metallurgy, and condensed matter physics for a long time.[8–12] While Landau's celebrated theory[15] of continuous phase transitions has successfully classified the phenomenology of symmetry breaking in the homogeneous random alloy upon ordering, actual predictions of phase stabilities were more often based on intuitive chemical and metallurgical constructs such as electronegativities,[8] electron concentrations,[9] atomic sizes,[10,11] and orbital radii.[12] Of particular interest to us here are the approaches that attempt to demystify structural selectivity directly in terms of the electronic structure. In this respect, recent advances in first-principles self-consistent formulations of the total electron and ion energies of solids[16] have produced a wealth of information on the ground-state properties of *ordered* intermetallic and semiconducting compounds. Given the crystal structure type of an ordered compound, one can calculate its equilibrium lattice parameters, elastic constants, phonon frequencies, and cohesive energy, often within a few percent of the measured values.[16] To find the stable crystal configuration, one then repeats the total energy calculation for a few other assumed crystal structures that by analogy with related compounds are expected to be likely competitors for the stable ground state. Comparison of total-energy–versus–volume curves for such a set of "intuitive structures" permits the identification of the stablest structure in this set and possible phase interconversions among them. While generally successful, the predictive value of this approach does depend on one's ability to guess correctly a canonical set of structures which includes the "winning" (minimum-energy) configuration. One wonders, however, whether a different, hitherto unexpected structure could have yet lower energy, or whether linear combination of two other structures with compositions x_α and x_β (and $x_\alpha < x_\sigma < x_\beta$) could have a lower energy than σ (hence, σ will disproportionate into α plus β). Addressing this problem, even for binary $A_n B_{N-n}$ compounds requires, in principle, calculation of the total energies of the 2^N atomic configurations for each type of lattice (fcc, bcc, . . .) with N lattice sites per cell. Even limiting N to

$O(10)-O(10^2)$, this is a formidable task for first-principles electronic structure methods, where the effort involved in obtaining the total energy of a *single* configuration scales as $(MN)^3$, where M is the number of orbitals/atom used to expand the single-particle wave functions. While lattice theories of statistical mechanics[17-25] provide an effective means of searching for the ground-state configuration within model (e.g., Ising-type) Hamiltonians, this approach has often evolved around the limited task of identifying the Hamiltonian parameters that produce *given* phase phenomena, rather than explaining them in terms of a microscopic theory of electronic structure.

In this paper we demonstrate how one can effectively identify the ground-state structures among many $[O(2^N)]$ atomic configurations directly from a microscopic electronic structure theory, using the (quantum-mechanical) calculated total energies of only ~ 10 crystal structures. The method is illustrated for the four intermetallic alloys of Fig. 1 and $Al_{1-x}Ni_x$. This establishes a direct link between the *ab initio* electronic structure theory and structural preferences in solids.

II. CLUSTER EXPANSION OF PROPERTIES OF BINARY LATTICES

The physical properties of various lattice configurations are often depicted by "cluster expansions" described by Sanchez *et al.*[25] These are formulated as follows. A binary lattice with N sites can exist in 2^N different configurations σ, corresponding to the various occupations of the N sites by the atoms A and B. Each configuration can be labeled by a set $\{\widehat{S}_i\}$ of fictitious spin variables $\widehat{S}_i$: $+1$ if site i is occupied by B, -1 if it is occupied by A. We will be interested in describing various physical properties $P(\sigma)$ of given configurations, e.g., its total (electron plus ion) energy $E(\sigma)$, equilibrium molar volume $V(\sigma)$, composition $X(\sigma)$, etc. While for periodic crystals with a reasonable small number of atoms per unit cell $P(\sigma)$ could be readily calculated (e.g., from band theory), the multitude of configurational and structural degrees of freedom characterizing either disordered or imperfectly ordered configurations renders the direct calculation of $P(\sigma)$ intractable.[26] Whereas one could calculate $P(\sigma)$ directly[26] for certain limited classes of configurations, the basis of lattice model[17-25] is to expand it instead in a series of contributions p_f of "figures" f and focus on the calculation of these elemental contributions p_f. A figure is defined as a cluster of atoms with k_f vertices (i.e., a selection of k_f out of N sites). The expansion is defined with respect to an orthonormal set of coefficients, as follows. One defines the spin product

$$\Pi_f(\sigma)=\widehat{S}_{1_f}\widehat{S}_{2_f}\cdots\widehat{S}_{k_f} , \qquad (2.1)$$

for each of the 2^N figures in configuration σ. The set $\{\Pi_f(\sigma)\}$ is orthonormal,[25] [including the "empty figure" $f=0$ for which $\Pi_0(\sigma)=1$] in that for two figures f and f' we have

$$\sum_\sigma \Pi_f(\sigma)\Pi_{f'}(\sigma)=2^N\delta_{f,f'} . \qquad (2.2)$$

Equation (2.2) shows that $2^{-N}\Pi_f(\sigma)$ is the inverse matrix of $\Pi_f(\sigma)$; multiplying the matrices in reverse order one obtains the second orthogonality condition between the two configurations σ and σ':

$$\sum_f \Pi_f(\sigma)\Pi_f(\sigma')=2^N\delta_{\sigma,\sigma'} . \qquad (2.3)$$

One can hence expand any property $P(\sigma)$ of the lattice configuration σ in the orthonormal set of $\{\Pi_f(\sigma)\}$ as[27]

$$P(\sigma)=\sum_f^{2^N} \Pi_f(\sigma)p_f , \qquad (2.4)$$

where the configuration-independent contribution p_f of figure f to the property P is given from Eqs. (2.2)–(2.4) by

$$p_f=2^{-N}\sum_\sigma^{2^N} \Pi_f(\sigma)P(\sigma) . \qquad (2.5)$$

The series (2.4) may be reduced using symmetry. Denoting by $\widehat{R}$ one of the N_L operations of the space group of the lattice (not the space group of a particular configuration σ) we have

$$P(\widehat{R}\sigma)=P(\sigma) \qquad (2.6)$$

and

$$\Pi_{\widehat{R}f}(\widehat{R}\sigma)=\Pi_f(\sigma) , \qquad (2.7)$$

hence, Eq. (2.5) gives

$$p_{\widehat{R}f}=p_f , \qquad (2.8)$$

so all ND_F symmetry-related figures contribute equally to $P(\sigma)$. This fact can be used to reduce the sum in Eq. (2.4) to just the symmetry-inequivalent figures F

$$P(\sigma)=N\sum_F \overline{\Pi}_F(\sigma)D_Fp_F , \qquad (2.9)$$

where the "lattice-averaged spin product' (denoted by an overbar) of the prototype figure F in configuration σ is

$$\overline{\Pi}_F(\sigma)=\frac{1}{N_L}\sum_{\widehat{R}}^{N_L}\Pi_{\widehat{R}F}(\sigma) , \qquad (2.10)$$

and N_L is the number of operations $\widehat{R}$ in the lattice space group (e.g., $N_L=48N$ for fcc lattices). The set of $\{\overline{\Pi}_F(\sigma)\}$ characterizes unequivocally the structure of configuration σ. Indeed, using the alternative definition to Eq. (2.10), and summing over the figures f that are symmetry related to F:

$$\overline{\Pi}_F(\sigma)=\frac{1}{ND_F}\sum_{f\in F}\Pi_f(\sigma) , \qquad (2.11)$$

one finds that

$$\sum_F D_F\overline{\Pi}_F(\sigma)\overline{\Pi}_F(\sigma')=\frac{2^N}{NN_L}\sum_{\widehat{R}}\delta_{\sigma,\widehat{R}\sigma'} \qquad (2.12)$$

which is the orthogonality condition between symmetry-unique configurations, analogous to Eq. (2.3).

The cluster expansion of Eq. (2.4) defines a multisite Is-

ing Hamiltonian[18] which includes "interactions" $p_F \equiv p_{k,m}$ between k pseudospins separated by up to the mth neighbor distance (the choice $k=2$, $m=1$ corresponds to the classic,[17,18] nearest-neighbor pair interaction case). Since the configurational property $P(\sigma)$ can depend in general on the external volume V (or pressure) of the lattice, so will the cluster contributions $\{p_f\}$.

It is useful to expand the configurational property $P(\sigma)$ with respect to some *reference configuration*. One possibility is to expand it relative to the property P of equivalent amounts of pure A and pure B lattices. The cluster expansions for $\sigma = A$ and $\sigma = B$ are

$$P(A,V) = \sum_m \sum_k (-1)^k D_{k,m} p_{k,m}(V) \qquad (2.13)$$

and

$$P(B,V) = \sum_m \sum_k (+1)^k D_{k,m} p_{k,m}(V) , \qquad (2.14)$$

since for pure A and pure B spin products of Eq. (2.1) are $+1$ for all k=even figures, while for k=odd they are -1 for $\sigma = A$ and $+1$ for $\sigma = B$ (see Tables III and IV below). Extracting from Eqs. (2.13) and (2.14) the value of $p_{k,m}$ for the "empty figure" $(k,m)=(0,1)$ and for the site-only (1,1) figure, and substituting them into Eq. (2.9) gives the *excess* property ΔP for the $A_{1-x}B_x$ system with respect to equivalent amounts of A and B

$$\Delta P(\sigma, V) \equiv P(\sigma, V) - [(1-x)P(A,V) + xP(B,V)] . \qquad (2.15)$$

The cluster expansion for ΔP is then

$$\Delta P(\sigma, V) = \sum_{m>0} \sum_{k>1} [\overline{\Pi}_{k,m} - \eta] D_{k,m} p_{k,m}(V) , \qquad (2.16)$$

where $\eta = 1$ for k=even and $\eta = (2x-1)$ for k=odd. Choosing alternatively the perfectly random (R) $A_{1-x}B_x$ alloy as a reference system, the ensemble average over the 2^N configurations (denoted by angular brackets) is

$$\langle \overline{\Pi}_{k,m} \rangle_R = (2x-1)^k . \qquad (2.17)$$

The excess energy of the perfectly random alloy is then

$$\langle \Delta P \rangle_R = \sum_{m>0} \sum_{k>1} [(2x-1)^k - \eta] D_{k,m} p_{k,m}(V) , \qquad (2.18)$$

so the cluster expansion can be written with respect to $\langle \Delta P \rangle_R$ as

$$\Delta P(\sigma, V) = \langle \Delta P \rangle_R$$
$$+ \sum_{m>0} \sum_{k>1} [\overline{\Pi}_{k,m}(\sigma) - (2x-1)^k] D_{k,m} p_{k,m} . \qquad (2.19)$$

While the complete cluster expansions of Eqs (2.4), (2.16), or (2.19) are formally exact, they merely replace a direct calculation of 2^N values of $P(\sigma)$ by an equivalent number of calculations of the elementary contributions p_f. The utility of these expansions rests, however, in the possibility of identifying a hierarchy of a small ($\ll 2^N$) number of figures whose contributions $p_{k,m}$ to the physi-

cal property P dominates those of the remaining figures. To the extent that this is possible, the full informational content of 2^N values of $P(\sigma)$ can be reduced to a smaller set of $\{p_F\}$ elementary interactions. These can then be used to predict $P(\sigma)$ for other structures,[27] to search among all 2^N configurations[19-23] for the $T=0$ "ground-state structure" (that has the lowest P=total energy), or to predict the finite-temperature thermodynamic properties of $A_{1-x}B_x$ through solution of the Ising problem[18,27] of Eq. (2.4).

There are qualitative indications that the cluster expansion might be reasonably rapidly convergent for a number of physical properties $P(\sigma)$. Note first that such expansions need to capture only the *difference* $\Delta P(\sigma)$ between the property $P(\sigma)$ of some structure $A_{1-x}B_x$ and the average property taken over equivalent amounts of its constituents A and B. Indeed, such differences are often much smaller than $P(\sigma)$ itself, e.g.: (i) for P=molar volume or lattice constant, Zen's and Vegard's rules[10] state, respectively, that $\Delta P \approx 0$; (ii) for P=total energy, the formation enthalpy ΔP is many orders of magnitude smaller[5,13,16(c)] than the total electron and ion energy of $A_{1-x}B_x$; and for (iii) P=optical band gap of semiconductors, the "optical bowing parameter" ΔP is usually less than[27(a),(b)] 10% of P. Similarly, comparing $\Delta P(\sigma)$ for some ordered configuration σ to its values $\langle \Delta P \rangle_R$ in the random alloy at the same composition [Eq. (2.19)] shows comparable trends, e.g., for (i) ΔP= formation enthalpy $\Delta P(\sigma) - \langle \Delta P \rangle_R$ is often ≤ 1 Kcal/mole for many intermetallics;[5] (ii) the changes in molar volume,[1,5,10] and (iii) optical band gaps[27] upon ordering of a random semiconductor alloy are often $\sim 1\%$. Second, note that the notion of the dominance of interactions between neighboring atomic sites over interactions between more distant sites underlines much of the phenomenological structural chemistry of intermetallic phases.[8-11] Theories of atom packing in lattices[28-35] retaining but the first few pair interactions have been eminently successful for many types of solids.

Many previous applications of the Ising-type Hamiltonian of Eq. (2.4) have not formulated $p_{k,m}$ through a microscopic theory. Instead, it was often postulated[19-23] that a given set of interactions describe some generic physical systems; nearest-neighbor pair interaction models are some of the popular idealizations of Eq. (2.4). Often, those interactions are adjusted to fit an observed phase diagram.[36-38] The general expansion (2.4) can, however, be made useful for predicting structural energies of solids to the extent that a reasonably rapidly convergent series of interaction $\{p_{k,m}\}$ can be calculated *a priori*. We next review the way in which these interactions were obtained previously.

III. THEORIES OF INTERACTION ENERGIES $\{p_{k,m}\}$

The expansion of the configurational energy of a molecule or solid in terms of pair and multiatom interactions has a long history in organic[30,31] and inorganic[30,34] chemistry, metallurgy,[28,33] physics of semiconductors[35] and ionic solids.[29,32] The interaction potentials are generally obtained there without reference to *lattice models:* they

are extracted, for example, through fits of the observed dissociation energies, molecular conformations, and vibrations,[30-32,34,35(a)] or fits of calculated[35(b),39] (e.g., by the Hartree-Fock[39] or density functional[35(b)] Born-Oppenheimer energy surfaces), or through pseudopotential perturbation expansions.[33] In many cases, $p_{k,m}$ is identified with interatomic interaction *potential*, not with averages over the *total* energies [Eq. (2.5)]. A classic example that serves to emphasize this distinction is the Madelung (M) energy[32] of a lattice configuration σ

$$E_M(\sigma) = \frac{1}{2N} \sum_{ij}{}' \frac{Q_i Q_j}{|\mathbf{R}_i - \mathbf{R}_j|} ,$$ (3.1)

where the prime excludes the $i = j$ term and the pair interaction potential

$$\tilde{p}_{i,j} = \frac{Q_i Q_j}{|\mathbf{R}_i - \mathbf{R}_j|} \hat{S}_i \hat{S}_j$$ (3.2)

is the Coulomb interaction between point charges Q_i and Q_j on lattice site $\mathbf{R}_i$ and $\mathbf{R}_j$. As is well known,[32] this series converges both slowly and conditionally due to the slow decay of $\tilde{p}_{i,j}$ (unless one is summing over carefully selected neutral clusters of sites). In contrast, the cluster expansion considered in this paper [Eqs. (2.4) and (2.5)] identifies the cluster parameters $p_{k,m}$ with interaction *energies* that renormalize a set of (possibly long-ranged) potentials. In the context of the Madelung problem, the effective interaction energies of Eq. (2.4) take the form (2.5)

$$p_{2,m} = 2^{-N} \sum_{\sigma}^{2^N} \Pi_{2,m}(\sigma) E_M(\sigma) ,$$ (3.3)

representing an average over configurations of converged lattice sum $E_M(\sigma)$. Hence, the (renormalized) effective interaction energies $\{p_{k,m}\}$ can be of considerably shorter range than conventional interaction potential $\{\tilde{p}_{k,m}\}$. This is illustrated in Sec. IV E below.

The empirical approach of extracting $\{p_{k,m}\}$ from experimental data has also been used extensively in the context of lattice models of phase diagrams. There, one first truncates the cluster expansion to a given range, and adjusts $\{p_{k,m}\}$ in the solution of the corresponding Ising model of Eq. (2.4) to reproduce certain features (e.g., transition temperatures) of the experimental phase diagrams. Examples include the fit of Kikuchi *et al.*[36] of Cu-Ag-Au phase diagrams to a nearest-neighbor Ising model $(m = 1, k \leq 4)$ solved through the cluster-variation method (CVM), the fit of Sigli and Sanchez[37] of $Al_{1-x}Ni_x$ phase diagram through a nearest-neighbor pair model, and a similar fit by Sanchez *et al.*[38] using the nearest-neighbor Lennard-Jones form for $p_{k,1}$. While good fits can be obtained within nearest-neighbor models,[36-38] the extent to which these empirical interactions renormalize longer-range terms remains unknown, as is their physical interpretation. These interaction energies can also be estimated directly from x-ray- or neutron-diffuse-scattering measurements, as done, for example, by Cenedese *et al.*[40] for $Al_{1-x}Ni_x$ and $Fe_{1-x}Ni_x$.

In contrast with the *classical* empirical interaction po-

tentials discussed above which circumvent altogether the consideration of the (quantum-mechanical) electronic degrees of freedom, the embedded-atom model[41,42] (EAM) describes configurational energies in terms of electron-density-mediated interatomic energies. There, $E(\sigma)$ is expanded in terms of a sum over single-site $(k = 1, m = 0)$ terms, each representing the energy of embedding atom i in an electron bath of density ρ_i, and a set of pair-interaction terms. The site charge density ρ_i includes the configuration-dependent effect of the charge densities of the surrounding atoms; embedding energies are described within the density functional model, e.g., through the quasiatom approach of Stott and Zaremba[43] or the effective medium approach of Nørskov and Lang.[44] In many practical applications[41,42] the parameters of the electron densities, two-body potentials, and the embedding functions are adjusted to fit experimental data (e.g., equilibrium lattice constants, cohesive energies, vacancy formation enthalpies, bulk and shear moduli).

A direct quantum-mechanical approach to calculating interaction energies within the lattice model is provided by the definition of Eq. (2.5). In practical calculations, the number of configurations included in the sum are restricted to $O(10)$–$O(10^2)$, and $P(\sigma) = E(\sigma)$ is evaluated within simple non-self-consistent tight-binding models. Applications of this "direct configurational average" (DCA) method[45] showed that (within the limitations of an inherently short-ranged electronic Hamiltonian), the pair interactions $\{p_{2,m}\}$ describing model binary transition metal alloys converge rapidly with the cluster size m.

Current quantum-mechanical approaches to calculating effective interaction energies—the "concentration wave" (CW) method[46-51] and the "generalized perturbation method"[52-57] (GPM)—are based on expanding $\Delta P(\sigma, V)$ relative to the random alloy average $\langle \Delta P \rangle_R$ [Eq. (2.19)] *without* expanding the latter quantity in a cluster from [Eq. (2.18)]:

$$\Delta E(\sigma) = \langle \Delta E(x) \rangle_{\mathrm{SCPA}} + \frac{1}{2} \sum_{ij} V_{ij}^{(2)}(x_i - x)(x_j - x)$$

$$+ \frac{1}{3} \sum_{ijk} V_{ijk}^{(3)}(x_i - x)(x_j - x)(x_k - x) + \cdots .$$ (3.4)

Here, the energy of the random alloy is calculated independently from an electronic Hamiltonian that is explicitly configurationally averaged, using the site coherent potential approximation[50] (SCPA), while $V^{(k)}$ are effective k-body potentials and x_i is the concentration of atom B on site i. In the "concentration wave" approach,[46-51] $V_{ij}^{(2)}$ is obtained from the derivative of the inhomogeneous CPA energy

$$V_{ij}^{(2)} = \frac{\partial^2 \langle E\{x_i\} \rangle_{\mathrm{CPA}}}{\partial x_i \partial x_j} ,$$ (3.5)

whereas in the "generalized perturbation method"[52-57] the effective energies are obtained from a spectral integral of transfer matrices and Green's functions.[53] The SCPA energy $\langle E \rangle_{\mathrm{SCPA}}$ common to both approaches was formulated either within the tight-binding[52-57] or the muffin-tin Korringa-Kohn-Rostoker (KKR) formalism.[47-51] In the former case, the total energy includes but the sum of

single-particle energies (the "band-structure" term), while in the latter case "double counting" (electron-electron Coulomb and exchange-correlation) terms could[51] be included.

The self-consistent KKR-CPA total energy $\langle \Delta E \rangle_{CPA}$ of the random alloy (including both band structure and double-counting terms) has been calculated for fcc $Cu_{1-x}Zn_x$ alloys,[51] yielding the composition-dependent equilibrium lattice constant $a(x)$, in good agreement with experiment. The effective interactions, obtained for $Pd_{1-x}Rh_x$ (Ref. 49) and $Cu_{1-x}Pd_x$ (Ref. 48) were calculated, however, from the one-electron band-structure terms, neglecting charge transfer, atomic relaxation, variation of the total energy with respect to volume, and nonspherical terms in the atomic potentials. Despite this, the calculated $Pd_{1-x}Rh_x$ phase diagram[49] (using ideal mixing entropy) and the short-range order diffuse scattering map[49] are in qualitatively good agreement with experiment.

The CPA-GPM approach[52−57] has been applied within the non-self-consistent tight-binding d band model to a large number of transition metal binary alloys, yielding (i) predictions for fcc and bcc ground-state structures[54] and phase diagrams[56] in terms of tight-binding constructs such as d electron count per atom and d band widths, (ii) formation enthalpies of ordered and disordered alloys,[57] (iii) predictions of relative stabilities of different ordered structures at the same composition[55,56] (e.g., $L1_2$ and DO_{22}), and (iv) predictions of effective cluster interactions,[54−56] exhibiting a rather fast convergence as a function of the cluster size. Extensions in which the tight-binding Hamiltonian is replaced by a KKR form within the CPA-GPM were also reported.[58]

Methods that are based on Eq. (3.4), e.g., the CPA-GPM or CPA-CW rely fundamentally on the adequacy of the SCPA approach to the description of the total energy of the random system and perturbations thereof. All such applications to date[47−57] are based on the implementation of the CPA within the site-only approximation.[50] This approach amounts to assuming that at a fixed composition the properties of an atomic site in the alloy (e.g., electronic charge, local density of states, self-consistent potential) do not depend explicitly on the configuration of the surrounding atoms, including its first nearest neighbors. The simulations of the electronic structure of random configurations by Alben et al.,[58] Davis et al.,[59] and Gonis et al.[60] demonstrated, however, significant local environment effect on the density of states. In actuality, this electronic inequivalence between chemically identical species in the alloy (i.e., the different A sites in a random configuration) would create nonvanishing forces about the atoms, driving positional relaxations. The existence of a distribution of local charges would also set-up a finite Madelung energy for the random alloy. In short, the electronic "glue" creates about each site a "sphere of influence," whereby the structural and chemical information associated with the atoms in this sphere affect the local properties of the central atom. The SCPA replaces this "sphere of influence" by a point. The local density of states and total energy of such a configuration is evaluated by replacing the distribution of

many inequivalent local environments by a *uniform medium,* having the high symmetry of the *empty* lattice and vanishing Madelung energy. There are but two distinct average potential functions in the problem (one for A, one for B); all A atoms (and separately, all B atoms) are taken to be electronically equal. Hence, in averaging over all local environments to produce an effective medium, the SCPA removes all *geometrical* aspects of the problem (e.g., the particular way in which an atom is coordinated to a certain number of neighbors), retaining but the *topology* (i.e., the correct coordination symmetry underlying the Bravais lattice of the pure constituents). The present authors find this approximation to be physically implausible for systems with significantly different A versus B bonding properties (e.g., sizes, ionicities, or scattering strengths). We will further demonstrate this point in Sec. IV E. We find there [Eq. (4.24)] that setting the random Madelung energy to zero, as assumed by the SCPA makes a 100% error in the electrostatic contribution to the ordering energy. In what follows, we will hence cluster expand the energy of the random alloy [Eq. (2.18)] and that of ordered structures [Eq. (2.16)] in a precisely equivalent manner, avoiding single-site effective medium averaging. We next demonstrate how the cluster properties $p_{k,m}$ can be obtained from the configurational properties $\{P(\sigma)\}$ of a subset of distinct configurations.

IV. CALCULATION OF EFFECTIVE CLUSTER PARAMETERS $p_{k,m}$ FROM $P(\sigma)$

A. Formalism

To the extent that the basic cluster expansion of Eq. (2.9) converges regularly and rapidly with respect to the figures $\{F\}$ (a point examined below), one can use *any* sufficiently large set of $\{P(\sigma)\}$ in Eq. (2.9) to evaluate the effective cluster properties $\{p_F\}$. Conversely, nonunique values of $\{p_F\}$ obtained from two different sets of configurations $\{\sigma\}$ and $\{\sigma'\}$ of comparable sizes testify to the importance of interactions beyond the truncation limit used. This suggests that one can (i) establish a trial maximum figure F_{max} to be retained in the cluster expansion of Eq. (2.9), (ii) select a computationally *convenient* set of configuration $\{\sigma\}$ (e.g., periodic structures) from which p_F for $F \leq F_{max}$ can be obtained, and (iii) examine convergence by using $\{p_F\}$ to predict the property $P(\sigma')$ for *other* structures $\{\sigma'\} \neq \{\sigma\}$; if this fails, F_{max} is increased until transferability is established.

Following Connolly and Williams[61] we specialize the expansion of Eq. (2.9) to a set of N_s *periodic structures* $\{\sigma\} = \{s\}$ for which (i) $P(\sigma)$ can be readily calculated (e.g., from band theory) and (ii) $\{\overline{\Pi}_F(s)\}$ are known trivially. This reads

$$P(s, V) = N \sum_F^{F_{max}} \overline{\Pi}_F(s) D_F p_F \ . \tag{4.1}$$

One then obtains the effective cluster properties $\{p_F\}$ either through matrix inversion (if N_s equal the number N_F of figures used), as suggested by Connolly and Williams[61]

$$p_F = \frac{1}{ND_F} \sum_s^{N_s} [\overline{\Pi}_F(s)]^{-1} P(s) , \tag{4.2}$$

or (if $N_F < N_s$) by minimizing the weighted variance,

$$\sum_s^{N_s} \omega_s \left[P(s) - \sum_F^{N_F} \overline{\Pi}_F(s) D_F p_F \right]^2 = \text{minimum} , \tag{4.3}$$

with the weights

$$\omega_s = 48 N_C(s) / N_G(s) . \tag{4.4}$$

Here $N_C(s)$ and $N_G(s)$ are the number of atoms per unit cell and number of point group operations for the structure s, respectively. An immediate consequence of Eqs. (4.1) and (4.2) is that if the contributions of clusters with $F > F_{max}$ can be neglected, the property $P(\sigma)$ of an arbitrary configuration σ can be represented as a superposition of the properties $\{P(s)\}$ of a set of ordered structures, i.e.,

$$P(\sigma) = \sum_s^{N_s} \xi_s(\sigma) P(s) , \tag{4.5}$$

where the weights are

$$\xi_s(\sigma) = \sum_F^{F_{max}} [\overline{\Pi}_F(s)]^{-1} \overline{\Pi}_F(\sigma) . \tag{4.6}$$

Note that $\{P(s)\}$ of Eqs. (4.3) or (4.5) could be calculated for *any* configuration s (including, if one wishes, "random" configurations) as long as $P(s)$ can be calculated accurately (e.g., without the site-only decoupling). In practice, one would seek to establish a sufficiently small set of representative configurations (see below), and judge its adequacy by the extent to which the interaction parameters extracted from it are transferable to the description of other configurations.

This method of "superposition of periodic structures" [Eqs. (4.5) and (4.6)] has been used by a number of authors, restricting, however, F_{max} to the nearest-neighbor figures. Within this approximation (to be examined below), there are only five nonequivalent values of $f = (k,m)$, i.e., $m = 1$ and $k = 0, 1, 2, 3$, and 4; the maximum figure F_{max} is the $A_n B_{4-n}$ tetrahedron with $0 \leq n \leq 4$. Applications of this nearest-neighbor model to P=total energy of bulk alloys include the work of Connolloy and Williams,[61] Terakura et al.[62(a)] and Takizawa and Terakura[62(b)] on transition metal alloys, that of Sanchez and Carlsson,[63(a)] and Carlsson[63(b)] on $Al_{1-x}Ni_x$, that of Sluiter et al.[63(c)] on LiAl, of Srivastava et al.,[64] Mbaye et al.,[65,66(a)] and Ferreira et al.[67] on semiconductor alloys, and the work of Wei et al.[68] on noble metal alloys. Applications to *epitaxial alloys* were reported by Mbaye et al.,[66(a)] and by Wood and Zunger.[66(b)] All of these applications evaluated $P(s) = E_{tot}$ using first-principles electronic structure techniques. Applications to P=band gaps include the work of Bernard and Zunger[69(a)] on II-VI semiconductor alloys, Wei and Zunger[69(b)] and Ling and Miller[70] on III-V semiconductors alloys. Application to P=spin-orbit splittings were carried out by Chadi[71] and by Wei and Zunger.[72] Finally,

application to P=*bond lengths* in semiconductor alloys were carried out by Balzarotti et al.,[73] Letardi et al.,[74] Sasaki and Ichimura,[75] Martins and Zunger,[76] and Wei and Zunger.[69(b)]

Extension of the "superposition of periodic structures approach" of Eqs. (4.1) and (4.2) to include a *converged* set of figures (e.g., up to fourth neighbors in fcc systems) was presented by Ferreira et al.[27(a)] and by Wei et al.[27(b)] for different II-VI and III-V semiconductor alloys, and by Lu et al.[27(c)] on transition metal alloys. Such larger, converged representations of the cluster expansion are considered next.

B. Selection of structures and figures

We see that there are two distinct convergence issues in this approach: (i) the truncation of the sum over figures in Eq. (4.1) to $F \leq F_{max}$ and (ii) the truncation of the number of structures in Eq. (4.2) or (4.3) after N_s terms. Note that the concentration wave method,[46,47] and the generalized perturbation method[52–57] encountered only the first of these two convergence problems.

Our previous studies[27] showed that one must start first with a rather large set of figures and reduce their number on the basis of convergence tests. In addition to the normalization figure $(k,m) = (0,1)$ and the single-site figure $(k,m) = (1,1)$, we will use a hierarchical set of *pair* interactions $(2,m) = (2,1)$, (2,2), (2,3), (2,4) for first, second, third, fourth fcc neighbors, respectively (fifth for bcc), as well as the three-body $(k,m) = (3,1)$ and four-body (4,1) terms. These $N_F = 8$ figures are defined in Table II; Fig. 2 depicts them graphically.[77] This is the most extensive set of cluster interactions used to date in first-principles calculations of metal alloys.

Regarding the set of N_s periodic structures $\{s\}$, the choice must be such that different sets of structures $\{s\} \neq \{s'\}$ must yield through Eq. (4.2) or (4.3) similar interaction parameters $\{p_F\}_s$ and $\{p_F\}_{s'}$, hence, reproduce $P(\sigma)$ of an arbitrary structure with equivalent precision. Note that, depending on the properties described, the
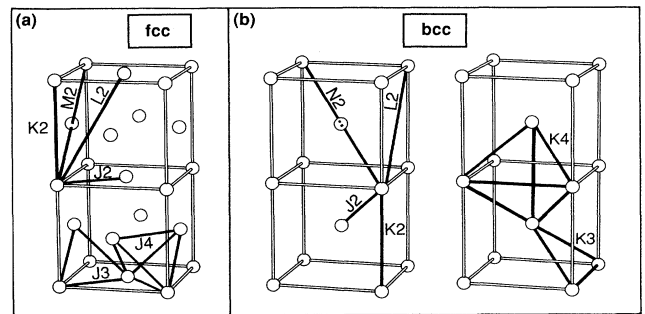

FIG. 2. Real-space depiction of the figures (Table II) used in the cluster expansion. (a) fcc and (b) bcc. Here, $J2 \equiv J_{2,1}$, $K2 \equiv J_{2,2}$, $L2 \equiv J_{2,3}$, $M2 \equiv J_{2,4}$, $N2 \equiv J_{2,5}$, $J3 \equiv J_{3,1}$, $K3 \equiv J_{3,2}$, $J4 \equiv J_{4,1}$, and $K4 \equiv J_{4,2}$.

cluster expansion permits (but does not require) that p_F depend on composition: the situation here is analogous to the expansion of a wave function $P(\sigma)$ by a finite set of (obviously nonunique) basis orbitals p_F that could, but need not depend on an energy parameter. We have previously shown[27] how an optimal set of structures can be selected so as to avoid any near-linear dependence (i.e., obtain a numerically stable inverse matrix $\overline{\Pi}_F^{-1}$). In the
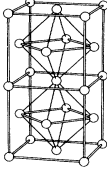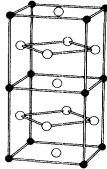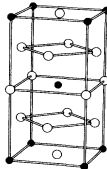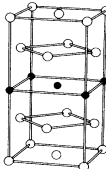
SB Name: (other)	A1,(fcc)	L1$_2$	DO$_{22}$	(β1, β2)
Formula:	A; B	A$_3$B ; AB$_3$	A$_3$B ; AB$_3$	A$_2$B ; AB$_2$
Crystal Structure ○A ●B				
Example	Cu	Cu$_3$Au	TiAl$_3$	
Bravais Lattice	Face-centered Cubic	Simple Cubic	Body-centered Tetragonal	Body-centered Tetragonal
Unit	(0,1/2, 1/2)	(1, 0, 0)	(1, 0, 0)	(1/2, 1/2, 0)
Cell	(1/2, 0, 1/2)	(0, 1, 0)	(0, 1, 0)	(1/2, -1/2, 0)
Vectors	(1/2,1/2, 0)	(0, 0, 1)	(1/2, 1/2, 1)	(1/2, 0, 3/2)
Space Group:				
Int. Tables:	Fm$\overline{3}$m	Pm$\overline{3}$m	I4/mmm	I4/mmm
Shoenflies:	O$_h^5$	O$_h^1$	D$_{4h}^{17}$	D$_{4h}^{17}$
Number:	225	221	139	139
Pearson Symbol:	cF4	cP4	tI8	tI6
Equivalent Superlattice	None	None	A$_3$B along [201]	A$_2$B$_1$ along [001]

SB Name: (other)	L1$_0$	L1$_1$	(CH, "40")	(Z2)
Formula:	A B	A B	A$_2$B$_2$	A$_2$B$_2$
Crystal Structure ○A ●B				
Example	CuAu-I	CuPt	NbP	
Bravais Lattice	Simple Tetragonal	Rhombohedral (Triagonal)	Body-centered Tetragonal	Simple Tetragonal
Unit	(1/2, 1/2, 0)	(1/2,1/2, 1)	(1, 0, 0)	(1/2,1/2, 0)
Cell	(-1/2, 0 ,1/2)	(1,1/2, 1/2)	(0, 1, 0)	(-1/2,1/2, 0)
Vectors	(0, 0, 1)	(1/2, 1, 1/2)	(1/2,1/2, 1)	(0, 0, 2)
Space Group:				
Int. Tables:	P4/mmm	R$\overline{3}$m	I4$_1$/amd	P4/nmm
Shoenflies:	D$_{4h}^1$	D$_{3d}^5$	D$_{4h}^{19}$	D$_{4h}^7$
Number:	123	166	141	129
Pearson Symbol:	tP4	hR32	tI8	tP8
Equivalent Superlattice	A$_1$B$_1$ along [001]	A$_1$B$_1$ along [111]	A$_2$B$_2$ along [201]	A$_2$B$_2$ along [001]
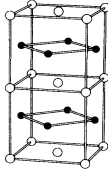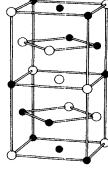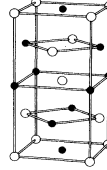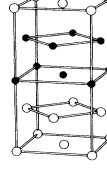
FIG. 3. Crystal structure information for the fcc compounds used in the cluster expansion. Table III gives the lattice-averaged spin products $\overline{\Pi}_{k,m}$ for these structures. In cases where a *structurbereicht* (SB) symbol is unavailable, we have made one up (given on top).

LU, WEI, ZUNGER, FROTA-PESSOA, AND FERREIRA

present study we have used 12 fcc and 12 bcc structures that satisfy the above conditions. They are shown in Figs. 3 and 4 that also give the unit cell vectors, Bravais lattices, space groups, and structure-type symbols. In cases where a structure-type symbol is unavailable in the literature we use our own labels. Tables III and IV give the lattice-averaged spin products $\overline{\Pi}_{k,m}(s)$ and degeneracies $D_{k,m}$ [Eq. (2.12)] ($D_{0,1}$ is set, for convenience, to uni-

SB Name: (other)	A2,(bcc)	DO$_3$	L6$_0$	C11$_b$
Formula:	A ; B	A$_3$B ; AB$_3$	A$_3$B ; AB$_3$	A$_2$B ; AB$_2$
Crystal Structure ○ A ● B				
Example	W	Bi F$_3$, Cs$_3$Sb	Cu Ti$_3$	MoSi$_2$
Bravais Lattice	Body Centered Cubic	Face Centered Cubic	Simple Tetragonal	Body - Centered Tetragonal
Unit	(-1/2, 1/2, 1/2)	(0, 1, 1)	(1, 0, 0)	(1, 0, 0)
Cell	(1/2, -1/2, 1/2)	(1, 0, 1)	(0, 1, 1)	(0, 1, 0)
Vectors	(1/2, 1/2, -1/2)	(1, 1, 0)	(0, -1, 1)	(1/2, 1/2, 3/2)
Space Group: Int. Tables	Im$\overline{3}$m	Fm$\overline{3}$m	P4/mmm	I4/mmm
Shoenflies:	O$_h^9$	O$_h^5$	D$_{4h}^1$	D$_{4h}^{17}$
Number:	229	225	123	139
Pearson Symbol:	cI2	cF16	tP4	tI6
Equivalent Superlattice	None	A$_3$B$_1$ along [111]	None	A$_2$B$_1$ along [001]

SB Name: (other)	B2	A$_1$	B32	B11
Formula:	A B	A B	A$_2$B$_2$	A$_2$B$_2$
Crystal Structure ○ A ● B				
Example	CsCl	γ-IrV	NaTl	γ-TiCu
Bravais Lattice	Simple Cubic	Centered Orthorombic	Face-centered Cubic	Simple Tetragonal
Unit	(1, 0, 0)	(1/2, 1/2, 1/2)	(0, 1, 1)	(1, 0, 0)
Cell	(0, 1, 0)	(1/2, -1/2, 1/2)	(1, 0, 1)	(0, 1, 0)
Vectors	(0, 0, 1)	(-1, 0, 1)	(1, 1, 0)	(0, 0, 2)
Space Group: Int. Tables:	Pm$\overline{3}$m	Cmmm	Fd$\overline{3}$m	P4/nmm
Shoenflies:	O$_h^1$	D$_{2h}^{19}$	O$_h^7$	D$_{4h}^7$
Number:	221	65	227	129
Pearson Symbol:	cP2	oC8	cF16	tP4
Equivalent Superlattice	A$_1$B$_1$ along [001]	A$_1$B$_1$ along [101]	A$_2$B$_2$ along [111]	A$_2$B$_2$ along [001]

FIG. 4. Crystal structure information for the bcc compounds considered in the cluster expansion. Table IV gives the lattice-averaged spin products $\overline{\Pi}_{k,m}$ for these structures. In cases where a *structurbereicht* (SB) symbol is unavailable, we have made one up (given on top).

TABLE II. Definition of the basic figures in the fcc and the bcc lattices and their degeneracies D_F. We use the lattice parameter $a = 2$. See Fig. 2 for a real-space representation of these figures.

Figure symbol	fcc D_F	fcc Site positions (in units of $a=2$)	bcc D_F	bcc Site positions (in units of $a=2$)
(0,1)	1	Empty	1	Empty
(1,1)	1	(0,0,0)	1	(0,0,0)
(2,1)	6	(0,0,0),(1,1,0)	4	(0,0,0),(1,1,1)
(3,1)	8	(0,0,0),(1,1,0),(1,0,1)		
(3,2)			12	(0,0,0),(1,1,1),(1,1,−1)
(4,1)	2	(0,0,0),(1,1,0),(1,0,1),(0,1,1)		
(4,2)			6	(0,0,0),(1,1,1),(1,1,−1),(2,0,0)
(2,2)	3	(0,0,0),(2,0,0)	3	(0,0,0),(2,0,0)
(2,3)	12	(0,0,0),(2,1,1)	6	(0,0,0),(2,2,0)
(2,4)	6	(0,0,0),(2,2,0)		
(2,5)			4	(0,0,0),(2,2,2)

ty) for these structures. Since we wish to use the same canonical set of structures and figure for all alloys studied here, we examine next how these sets predict, via the cluster expansion, *simple configurational properties* $P(\sigma)$ such as moments of composition, molar volumes, and Madelung energies. To the extent that a *single* set of structures and figures can be used to describe such a *range* of properties, the approach would be deemed both practical and physically appealing.

C. Cluster expansion of the moments of the composition

Equation (2.18) shows that the excess energy of a random alloy can be written as a power series of composition, where the coefficients of X^2, X^3, and X^4, for example, are determined primarily by pair, three-body, and four-body interactions, respectively. It is hence important that the general cluster expansion correctly capture the various powers X^λ of the composition, in particular the dominant $\lambda = 2$ (pair interaction) term. Using our set of $N_s = 12$ structures (Figs. 3 and 4) and $N_f = 8$ figures, we specialize Eq. (4.1) to $P(s) = X_s^\lambda$, i.e.,

$$X_s^\lambda = N \sum_F \overline{\Pi}_F(s) D_F x_F(\lambda) . \qquad (4.7)$$

Here, X_s^λ is the λth power of the composition of $X = m/(n+m)$ of the B atom in some structure $A_n B_m$. We determine the N_F expansion coefficients $p_F = x_F(\lambda)$ from N_s values of $P(s) = X_s^\lambda$ of the ordered structures $\{s\}$ by minimizing the variance of Eq. (4.3) (the cluster expansion reproduces identically the $\lambda = 0, 1$ moments). Table V compares for 12 fcc and 12 bcc structures the exact composition square X_s^2 with that recalculated by the cluster expansion, using the coefficients obtained from Eq. (4.7). We see that using this set of structures and figures reproduces X_s^2 rather accurately: the standard deviations χ are 0.009 and 0.008 for fcc and bcc lattices, respectively. The errors are larger for X_s^3 ($\chi = 0.021$ and 0.014 for fcc and bcc, respectively), but this would not affect seriously the calculated energies, as X^3 multiplies a rather small three-body term (Sec. V C below).

D. Cluster expansion of molar volumes

Another lattice property $P(\sigma)$ whose cluster expansion is physically relevant is the equilibrium molar volume $V(\sigma)$ of configuration σ. Using the linear-muffin-tin-orbital (LMTO) method[78] (described in Sec. V) we have minimized the total energies $\Delta E(s, V)$ of 12 fcc and 12 bcc ordered structures $\{s\}$ of AlNi compounds, finding for each (without any cluster expansion) the equilibrium volume

$$\frac{d\Delta E(s,V)}{dV}\bigg|_{V = V_{eq}^{(1)}(s)} = 0 . \qquad (4.8)$$

These directly calculated equilibrium volumes are denoted $V_{eq}^{(1)}(s)$. We then cluster expand, for $P(s) = V(s)$

$$V(s) = N \sum_F \overline{\Pi}_F(s) D_F v_F , \qquad (4.9)$$

obtaining the coefficients $p_F = v_F$ by minimizing the corresponding variance in Eq. (4.3). Inserting these expansion coefficients into Eq. (4.9) gives the recalculated volumes, denoted $V_{eq}^{(2)}(s)$. Finally, we calculate the volumes in a third way, by minimizing the cluster expansion for the *energies*

$$\frac{d\Delta E(s,V)}{dV} = N \sum_F \overline{\Pi}_F(s) D_F \frac{dJ_F(V)}{dV} = 0 , \qquad (4.10)$$

where $p_F = J_F$ are the expansion coefficient for the energy. This gives the equilibrium volume denoted $V_{eq}^{(3)}(s)$. Table VI compares these three equilibrium volumes, showing good agreement between them, and rapid convergence of the volume cluster expansion (4.9).

Equations (2.15) and (2.16) show that the normalization term $p_{0,1}$ and the site-only term $p_{1,1}$ give the linear part [second term on the right-hand side of Eq. (2.15)] of the property $P(\sigma)$, whereas the many-body terms $p_{k,m}$ with $k > 1$ and $m > 0$ describe deviations from linearity ["bowing" of $P(\sigma)$]. Table VII gives the expansion coefficients v_F of the volume series of Eq. (4.9) for the AlNi compounds, showing only small "bowing" of $V(x)$

LU, WEI, ZUNGER, FROTA-PESSOA, AND FERREIRA

TABLE III. Lattice-averaged $\overline{\Pi}_{k,m}(s)$ spin products and degeneracies $D_{k,m}$ for the 12 fcc structures used here. Figure 3 depicts these structures. The last column gives the configurational average $\langle \Pi_{k,m} \rangle = q^k$ for the random alloy, where $q = 2x - 1$.

Interaction		A1	$L1_2$	DO_{22}	$\beta1$	$L1_0$	$L1_1$	"40"	$Z2$	$\beta2$	DO_{22}	$L1_2$	A1	
$J_{k,m}$	$D_{k,m}$	A	A_3B	A_3B	A_2B	AB	AB	A_2B_2	A_2B_2	AB_2	AB_3	AB_3	B	Rand.
$J_0=J_{0,1}$	1	1	1	1	1	1	1	1	1	1	1	1	1	1
$J_1=J_{1,1}$	1	-1	$-\frac{1}{2}$	$-\frac{1}{2}$	$-\frac{1}{3}$	0	0	0	0	$-\frac{1}{3}$	$-\frac{1}{2}$	$-\frac{1}{2}$	1	q
$J_2=J_{2,1}$	6	1	0	0	$-\frac{1}{9}$	$-\frac{1}{3}$	0	$-\frac{1}{3}$	$-\frac{1}{3}$	$-\frac{1}{9}$	0	0	1	q^2
$J_3=J_{3,1}$	8	-1	$\frac{1}{2}$	$\frac{1}{2}$	$-\frac{1}{3}$	0	0	0	0	$-\frac{1}{3}$	$-\frac{1}{2}$	$-\frac{1}{2}$	1	q^3
$J_4=J_{4,1}$	2	1	-1	-1	1	1	-1	1	1	1	-1	-1	1	q^4
$K_2=J_{2,2}$	3	1	1	$\frac{2}{3}$	$\frac{5}{9}$	1	-1	$\frac{1}{3}$	$-\frac{1}{3}$	$\frac{5}{9}$	$\frac{2}{3}$	1	1	q^2
$L_2=J_{2,3}$	12	1	0	$-\frac{1}{3}$	$-\frac{1}{3}$	$-\frac{1}{3}$	0	$\frac{1}{3}$	$-\frac{1}{3}$	$-\frac{1}{3}$	$-\frac{1}{3}$	0	1	q^2
$M_2=J_{2,4}$	6	1	1	$-\frac{1}{3}$	$-\frac{1}{9}$	1	1	$-\frac{1}{3}$	$-\frac{1}{3}$	$-\frac{1}{9}$	$-\frac{1}{3}$	1	1	q^2

TABLE IV. Lattice-averaged spin products $\overline{\Pi}_{k,m}(s)$ and degeneracies $D_{k,m}$ for the 12 bcc structures used here. Figure 4 depicts these structures. The last column gives the configurational average $\langle \Pi_{k,m} \rangle = q^k$ for the random alloy, where $q = 2x - 1$.

Interaction		A2	DO_3	$L6_0$	$C11_b$	$B2$	A_1	$B32$	$B11$	$C11_b$	$L6_0$	DO_3	A2	
$J_{k,m}$	$D_{k,m}$	A	A_3B	A_3B	A_2B	AB	AB	A_2B_2	A_2B_2	AB_2	AB_3	AB_3	B	Rand.
$J_0=J_{0,1}$	1	1	1	1	1	1	1	1	1	1	1	1	1	1
$J_1=J_{1,1}$	1	-1	$-\frac{1}{2}$	$-\frac{1}{2}$	$-\frac{1}{3}$	0	0	0	0	$-\frac{1}{3}$	$-\frac{1}{2}$	$-\frac{1}{2}$	1	q
$J_2=J_{2,1}$	4	1	0	0	$-\frac{1}{3}$	-1	0	0	0	$-\frac{1}{3}$	0	0	1	q^2
$K_3=J_{3,2}$	12	-1	$\frac{1}{2}$	$-\frac{1}{6}$	$-\frac{1}{9}$	0	0	0	0	$-\frac{1}{9}$	$-\frac{1}{6}$	$-\frac{1}{2}$	1	q^3
$K_4=J_{4,2}$	6	1	-1	$-\frac{1}{3}$	$-\frac{1}{9}$	1	$-\frac{1}{3}$	1	$-\frac{1}{3}$	$-\frac{1}{9}$	$-\frac{1}{3}$	-1	1	q^4
$K_2=J_{2,2}$	3	1	0	$-\frac{1}{3}$	$\frac{5}{9}$	1	$-\frac{1}{3}$	-1	$-\frac{1}{3}$	$\frac{5}{9}$	$-\frac{1}{3}$	0	1	q^2
$L_2=J_{2,3}$	6	1	1	$-\frac{1}{3}$	$-\frac{1}{9}$	1	$-\frac{1}{3}$	1	$-\frac{1}{3}$	$-\frac{1}{9}$	$-\frac{1}{3}$	1	1	q^2
$N_2=J_{2,5}$	4	1	0	1	$-\frac{1}{3}$	1	1	-1	-1	$-\frac{1}{3}$	1	0	1	q^2

TABLE V. Comparison of the exact expectation values of the composition squared X^2 with the values obtained from the cluster expansion of Eq. (4.7) (using $N_F = 8$ and $N_s = 12$). The weights are given by Eq. (4.4). The crystal structures are shown in Figs. 3 (fcc) and 4 (bcc); Fig. 2 gives the figures (k, m) used. The last line gives the standard deviation.

Comp.	Exact X^2	fcc Struct.	fcc Weight	fcc Clust. X^2	bcc Struct.	bcc Weight	bcc Clust. X^2
A	0.0000	fcc	1	0.0000	bcc	1	0.0000
A_3B	0.0625	$L1_2$	4	0.0664	DO_3	4	0.0601
A_3B	0.0625	DO_{22}	12	0.0612	$L6_0$	12	0.0649
A_2B	0.1111	$\beta1$	9	0.0968	$C11_b$	9	0.1001
AB	0.2500	$L1_0$	6	0.2617	$B2$	2	0.2783
AB	0.2500	$L1_1$	8	0.2500	A_1	12	0.2476
A_2B_2	0.2500	"40"	12	0.2513	$B32$	4	0.2524
A_2B_2	0.2500	$Z2$	12	0.2643	$B11$	12	0.2610
AB_2	0.4444	$\beta2$	9	0.4301	$C11_b$	9	0.4334
AB_3	0.5625	DO_{22}	12	0.5612	$L6_0$	12	0.5649
AB_3	0.5625	$L1_2$	4	0.5664	DO_3	4	0.5601
B	1.0000	fcc	1	1.0000	bcc	1	1.0000
Deviation:				0.0089			0.0082

TABLE VI. Comparison of the equilibrium molar volume (in cm^3/g-at.) of $Al_{1-x}Ni_x$ intermetallic compounds as obtained by three different methods. $V^{(1)}(s)$ is obtained by minimizing the LMTO energy of structure s (no cluster expansion), $V^{(2)}(s)$ is obtained by cluster-expanding molar volumes using the 12 structures (Figs. 3 and 4) and 8 interactions (Fig. 2), and $V^{(3)}(s)$ is found by minimizing the corresponding *energy* cluster expansion with respect to volume. Note the good agreement between the cluster-expanded values $V^{(2)}$ and $V^{(3)}$ and the "exact" result $V^{(1)}$. Here, χ denotes standard deviation.

Structure	$V^{(1)}(s)$ [Eq. (4.8)]	$V^{(2)}(s)$ [Eq. (4.9)]	$V^{(3)}(s)$ [Eq. (4.10)]
	fcc		
fcc ($A = $Al)	9.595	9.595	9.595
$L1_2$ (A_3B)	8.258	8.276	8.298
DO_{22} (A_3B)	8.285	8.279	8.272
$\beta1$ (A_2B)	7.891	7.919	7.963
$L1_0$ (AB)	7.191	7.174	7.155
$L1_1$ (AB)	7.337	7.337	7.337
"40" (A_2B_2)	7.173	7.181	7.173
$Z2$ (A_2B_2)	7.479	7.478	7.456
$\beta2$ (AB_2)	6.861	6.835	6.744
DO_{22} (AB_3)	6.675	6.665	6.670
$L1_2$ (AB_3)	6.630	6.661	6.647
fcc ($B = $Ni)	6.343	6.343	6.343
χ	0	0.016	0.046
	bcc		
bcc ($A = $Al)	9.738	9.738	9.738
DO_3 (A_3B)	8.307	8.275	8.329
$L6_0$ (A_3B)	8.269	8.269	8.223
$C11_b$ (A_2B)	7.811	7.836	7.872
$B2$ (AB)	7.079	7.102	6.917
A_1 (AB	7.310	7.310	7.289
$B32$ (A_2B_2)	7.270	7.271	7.292
$B11$ (A_2B_2)	7.395	7.403	7.377
$C11_b$ (AB_2)	6.810	6.769	6.837
$L6_0$ (AB_3)	6.667	6.668	6.672
DO_3 (AB_3)	6.678	6.709	6.696
bcc ($B = $Ni)	6.397	6.397	6.397
χ	0	0.019	0.040

TABLE VII. The interactions $D_F v_F$ for the volume cluster expansion (in cm^3/g-at.) of Eq. (4.9) for Al$_{1-x}$Ni$_x$ compounds. $V^{(2)}(s)$ of Table VI are the equilibrium volumes obtained with these expansion coefficients.

Figure	fcc $V(s)$ series [Eq. (4.9)]	bcc $V(s)$ series [Eq. (4.9)]
(0,1)	7.355	7.374
(1,1)	−1.620	−1.618
(2,1)	0.521	0.121
(3,1)	−0.006	
(3,2)		−0.004
(4,1)	−0.048	
(4,2)		−0.005
(2,2)	0.066	0.051
(2,3)	0.076	0.014
(2,4)	−0.001	
(2,5)		0.001

(i.e., deviations from Vegard's rule), with $v_{2,1}$ being the leading nonlinear term. Among *pair* interactions, we see that the first neighbor term dominates, i.e.,

$$D_{2,1}v_{2,1} \gg D_{2,2}v_{2,2}, \ D_{2,3}v_{2,3}, \ D_{2,4}v_{2,4} \ . \qquad (4.11)$$

Regarding the many-body terms, we see that pair interactions dominate over the three- and four-body terms:

$$D_{2,1}v_{2,1} \gg D_{3,1}v_{3,1}, \ D_{4,1}v_{4,1} \ . \qquad (4.12)$$

Since the bowing in $V(x)$ is rather small, we will assume for the CuX compounds (X=Au, Pd, Pt, and Rh) the linear approximation. This is discussed further in Sec. V A.

E. Cluster expansion of electrostatic lattice energies

Since this paper focuses primarily on the cluster expansion of $P(\sigma)$=total lattice energy, it is of interest to find a closely related quantity for which exact analytical results are available, so the convergence of the expansion can be examined. Such a case is offered by the total *electrostatic* energy of a lattice of point charges [Eqs. (3.1) and (3.2)], i.e., the classic Madelung problem.

Evaluation of the Madelung energy[32] requires (i) modeling the distribution of point charges on the various lattice sites i occupied by (generally, crystallographically inequivalent) A and B atoms and (ii) summation of the electrostatic energies in Eq. (3.1) for a given model of point charge distribution. The choice of a model for a point charge distribution is generally nonunique; only in simple *ordered* binary AB compounds (e.g., CsCl) where there are just two inequivalent sublattices, one can make a unique choice $Q^{(B)}=-Q^{(A)}$ for all sites.

Consider first problem (i). As discussed in Sec. III, methods that are based on the SCPA approach (i.e., CPA-GPM[52−57] or CPA-CW[46−51] use a *single*-site decoupling of the configuration average in which only a single scatterer is treated exactly, while the rest are incorporated into an effective medium whose atoms are taken to be equal to one another. One is hence assuming there that

in an arbitrary random configuration the net charge Q_i on site i does not depend on the environment of this site; all A atoms are assumed to have the same net charge (and so do all B atoms). It then follows[79(b)] that the configuration average $\langle Q_i Q_j \rangle_R$ in Eq. (3.1) (appropriate to the random alloy) factors into the product $\langle Q_i \rangle_R \langle Q_j \rangle_R$ which is zero [on account of global charge neutrality $\langle Q_i \rangle_R = 0$], hence, $\langle E_M(\sigma) \rangle \equiv 0$. Consider, however, a random distribution of many A and B atoms on a fixed lattice. This will generally create various crystallographically inequivalent A sites (and separately, B sites) that are distinguished ·by different local atomic arrangements around them. It then seems reasonable to assume that an atom surrounded locally by atoms of the same chemical type would have a smaller net charge transfer than an atom surrounded, e.g., only by atoms of the opposite type. *Hence, a random occupation of sites need not lead to a random distribution of the physical properties of sites, e.g., charges.* We hence model the net charge Q_i to be proportional to the number of atoms of *opposite* type in the first coordination shell (containing Z_1 atoms):

$$Q_i = \lambda \sum_{k=1}^{Z_1} [\hat{S}_i - \hat{S}_k^{(i+1)}] \ , \qquad (4.13)$$

where $\hat{S}_i$ is the spin on site i, $\hat{S}_k^{(i+1)}$ is the spin on one of the Z_1 atoms that are nearest-neighbors to site i, and λ is a scaling constant determining the maximum charge transfer ($2Z_1\lambda$). This is not an arbitrary model: self-consistent calculations of Q_i for many ordered structures of Cu-Pd, Ag-Au, and Ag-Pd show[27(d)] a striking linear dependence of Q_i on the occupations of the nearest neighbors, in clear conflict with the SCPA. The charge distribution of Eq. (4.13) has the following properties: (i) the charges on A's and B's have opposite signs: different A sites (and different B sites) can have different charges reflecting variations in the local atomic arrangements; (ii) electroneutrality $\sum_i Q_i = 0$ is naturally satisfies; (iii) E_M of Eq. (3.1) is symmetrical with respect to the $A \leftrightarrow B$ replacement; and (iv) it reduces to the standard definition[79(a)] for prototype AB ordered lattices.

The Madelung energy per atom of Eq. (3.1) can be written for fcc-based structures s as

$$E_M(s) = \frac{-\alpha_M(s)(16\lambda)^2}{2R} \ , \qquad (4.14)$$

where $\alpha_M(s)$ is the Madelung constant, $R=a\sqrt{2}/2$, is the nearest-neighbor bond length and a is the cubic lattice constant in the fcc structure. Our model reduces to the standard definitions[32] for simple ordered compounds such as the $L1_0$ when $q \equiv 16\lambda$. We will next carry out a cluster expansion for $\alpha_M(s)$, evaluating from the electrostatic energy of the *random* alloy $\langle \alpha_M \rangle_R$. This will then be compared with the analytic results for $\langle \alpha_M \rangle_R$.

1. Cluster expansion of $\langle \alpha_M \rangle_R$

Using Ewald's method[79(a)] we have calculated the "exact" Madelung constant $\alpha_M(s)$ for our 12 canonical fcc ordered structures of Fig. 3, within the charge model of

Eqs. (4.13). The upper part of Table VIII (denoted "structures belonging to basis") gives the point charges obtained by this model and the "exact" Madelung constant $\alpha_M^E(s)$ obtained by applying Ewald's method to these structures. We then cluster-expand these $\alpha_M(s)$ using a set of pair-interactions $\{p_{2,m}\}$ with $m = 1, 2, 3, 4,$ and 5 (Since the Madelung energy represents *pair* interactions, all $k \neq 2$ interaction energies $p_{k,m}$ vanish. This increases the linear dependence of structures. In this case, out of the 12 canonical structures, only six of them are linearly independent.) Minimizing the variance of Eq. (4.3) yields[79(b)]

$$p_{0,1}^M = 0.736\,75, \quad p_{2,1}^M = -0.323\,93 ,$$

$$p_{2,2}^M = 0.083\,45, \quad p_{2,3}^M = 0.060\,93 ,$$

$$p_{2,4}^M = 0.034\,78, \quad p_{2,5}^M = 0.001\,39 . \qquad (4.15)$$

Note that this cluster expansion converges rapidly with the interatomic separation m, unlike the interaction potentials $\tilde{p}_{2,m}$ of Eq. (3.2). These effective cluster energies of Eq. (4.15) can then be used to calculate the Madelung constants using the cluster expansion (CE) of Eq. (4.1). The upper part of the Table VIII gives the recalculated Madelung constant $\alpha_M^{CE}(s)$.

To test the convergence of the cluster expansion for the Madelung energies, we now use Eqs. (4.5) and (4.6) along with the set of interaction energies (4.15) and *predict* $\alpha_M(s')$ for *additional* structures $\{s'\} = \{s\}$. The accuracy of these predictions can then be examined by comparing them to the Madelung constant $\alpha_M(s')$ calculated for these additional structures directly by Ewald's method. The additional structures $\{s'\}$ that we select can be described as superlattices whose layers are oriented in a given direction $\mathbf{G}$. We select a rather general set, corresponding to a range of ordering vectors $\mathbf{G}$:

$$Y2 = A_2B_2 \text{ with } \mathbf{G} = (1,1,0) ,$$

$$V2 = A_2B_2 \text{ with } \mathbf{G} = (1,1,1) ,$$

$$W2 = A_2B_2 \text{ with } \mathbf{G} = (1,1,3) ,$$

$$Z1, Z3 = A_3B \text{ and } AB_3 \text{ with } \mathbf{G} = (0,0,1) ,$$

$$Y1, Y3 = A_3B \text{ and } AB_3 \text{ with } \mathbf{G} = (1,1,0) , \qquad (4.16)$$

$$V1, V3 = A_3B \text{ and } AB_3 \text{ with } \mathbf{G} = (1,1,1) ,$$

$$W1, W3 = A_3B \text{ and } AB_3 \text{ with } \mathbf{G} = (1,1,3) ,$$

$$\alpha1, \alpha2 = A_2B \text{ and } AB_2 \text{ with } \mathbf{G} = (1,1,1) ,$$

$$\gamma_1, \gamma_2 = A_2B \text{ and } AB_2 \text{ with } \mathbf{G} = (1,1,0) .$$

The bottom half of Table VIII compares the Madelung constant $\alpha_M^E(s')$ of these additional "structure not in

TABLE VIII. This table gives, for various structures s, the point charges $Q_i^{(t)}(s)$ on atom t ($= A$ or B) at site i according to the model of Eq. (4.13) and their Madelung constant $\alpha_M(s)$ [Eq. (4.14)]. The top part of this table gives results for the 12 canonical fcc structures (Fig. 3) used in the cluster expansion of the Madelung energies. $\alpha_M^E(s)$ is the "exact" (E) Madelung constant calculated from Ewald's methods and $\alpha_M^{CE}(s)$ are the constants recalculated according to the cluster expansion (CE) using the coefficients extracted from these 12 structures. The bottom part of the table gives predictions of additional structures outside the set of 12, defined in Eq. (4.16). Note that these predictions compare very well with those obtained directly by Ewald's method for these additional structures. Structures A_nB_m and A_mB_n with the same symmetry have the same Madelung energy, hence we list only the A-rich member for each pair.

Structure s	$Q_1^{(A)}(s)$	$Q_2^{(A)}(s)$	$Q_1^{(B)}(s)$	$\alpha_M^E(s)$ (Ewald)	$\alpha_M^{CE}(s)$ (cluster expansion)
		Structures belonging to basis			
$A1$ (A)	0		0	0	0
$L1_2$ (A_3B)	-8λ		24λ	1.195 77	1.1958
DO_{22} (A_3B)	-8λ	-8λ	24λ	1.216 91	1.2169
$\beta1$ (A_2B)	-8λ		16λ	0.448 63	0.4486
$L1_0$ (AB)	-16λ		16λ	1.594 36	1.5944
$L1_1$ (AB)	-12λ		12λ	0.695 09	0.6951
"40" (A_2B_2)	-16λ		16λ	1.636 64	1.6366
$Z2$ (A_2B_2)	-8λ		8λ	$-0.135\,37$	-0.1354
		Structures not in basis			
$Y2$ (A_2B_2)	-12λ		12λ	0.588 82	0.5837
$V2$ (A_2B_2)	-6λ		6λ	$-0.240\,53$	-0.2434
$W2$ (A_2B_2)	-14λ		14λ	1.067 25	1.0635
$Z1$ (A_3B)	-8λ	0	16λ	0.330 91	0.3309
$Y1$ (A_3B)	-8λ	-4λ	20λ	0.693 00	0.6905
$V1$ (A_3B)	-6λ	0	12λ	0.053 51	0.0521
$W1$ (A_3B)	-6λ	-8λ	20λ	0.707 40	0.7055
$\alpha1$ (A_2B)	-6λ		12λ	0.072 07	0.0694
$\gamma1$ (A_2B)	-10λ		20λ	1.204 58	1.2029

basis" (calculated directly by Ewald's methods) with those predicted by the cluster expansion, using the coefficients of Eq. (4.15). The agreement is seen to be very good. We hence judge this expansion to be converged to within the error limit reflected in Table VIII.

Having established the convergence and transferability of the cluster expansion coefficients for Madelung constants, we can use Eq. (2.18) and predict the Madelung energy for the perfectly random (R) alloy. This gives, within the charge model of Eq. (4.13)

$$\alpha_M(R,x) = 4x(1-x) \times 0.7368 \quad (\text{for } N_s = 12) \qquad (4.17a)$$

using the 12 canonical structures and five effective pair interactions, or

$$\alpha_M(R,x) = 4x(1-x) \times 0.7392 \quad (\text{for } N_s = 27) \qquad (4.17b)$$

using in the basis *all* structures of Table VIII and six effective pair interactions.

2. Analytic results for $\langle E_M \rangle_R$

We next evaluate the Madelung energy analytically without using the cluster expansion, so that the precision of the latter can be evaluated. The configurational average of the Madelung energy, appropriate to a random alloy is

$$\langle E_M(\sigma) \rangle_R = \frac{1}{2N} \sum_{ij}' \frac{\langle Q_i Q_j \rangle_R}{R_{ij}}$$

$$= \frac{1}{2} \sum_{m}^{\infty} \frac{\langle Q_i Q_{i+m} \rangle_R}{R_m} Z_m \ , \qquad (4.18)$$

where Q_{i+m} is the charge on an atom in the mth shell (containing Z_m atoms) about the origin at i and R_m is the distance to the origin. Substituting our model (4.13) for the distribution of point charges into Eq. (4.18) gives

$$\langle E_M \rangle_R = \frac{\lambda^2}{2} \sum_{m=1}^{\infty} \frac{Z_m}{R_m} F_m(x) \ , \qquad (4.19)$$

where

$$F_1(x) = -4x(1-x)(2Z_1 - K_1) \ ,$$

$$F_{m>1}(x) = 4x(1-x)K_m \ , \qquad (4.20)$$

and K_m is the number of nearest-neighbor atoms shared by sites i and $i+m$. In an fcc lattice Z_m is 12, 6, 24, 12, 24, and 8 while K_m is 4, 4, 2, 1, 0, and 0 for shells $m = 1$, 2, 3, 4, 5, and 6, respectively. Note that $K_{m>5} = 0$, hence $F_{m>5} = 0$. From Eqs. (4.19) and (4.20) we have

$$\langle E_M(\sigma) \rangle = 4x(1-x) \frac{\lambda^2}{2} \left[-\frac{2Z_1^2}{R_1} + \sum_{m=1}^{4} \frac{Z_m}{R_m} K_m \right] \ .$$
$$(4.21)$$

Equating this to the definition of Eq. (4.14) then gives the analytical result

$$\alpha_M(R,x) = 4x(1-x) \times 0.739\,518\,2\ldots \ . \qquad (4.22)$$

This analytic result should be compared to that of the truncated cluster expansion [Eq. (4.17)]: the agreement is seen to be excellent; using more than six interactions improves this rapidly.

3. Discussion of the Madelung energies

In the remainder of this paper we will apply the same cluster expansion procedure used above for the Madelung energies (Sec. IV E 1) to calculate the total electron plus ion energies. In the latter case, analytic results are not available for comparison. However, the agreement found here between the truncated cluster expansion and the analytic results for the Madelung lattice, lend credence to this general procedure. Observe, in particular, that despite the long range of the *bare* Coulomb interactions $\tilde{p}_{ij}$ of Eq. (3.2), the *renormalized* interactions used throughout this paper [e.g., Eq. (3.3) and (4.15)] are of considerably shorter range, leading to a rapid convergence of the cluster expansion.

Our results $E_M(R) \neq 0$ [Eqs. (4.14) and (4.22)] should be contrasted with $E_M(R) \equiv 0$ assumed by all models that are based on the homogeneous SCPA. The contribution of the Madelung energy to the "ordering energies"

$$\Delta E_M^{\text{ord}} = E_M(s) - E_M(R) \qquad (4.23)$$

are given in Eq. (4.24) in units of $(16\lambda)^2/2R$; we give in parentheses the values corresponding to the SCPA:

$$
\begin{aligned}
&L1_0 \text{:} -0.8549 \ (-1.5944) \ , \\
&L1_1 \text{:} +0.0444 \ (-0.6951) \ , \\
&\text{``40'':} -0.8970 \ (-1.6366) \ , \\
&Z2 \text{:} +0.8749 \ (+0.1354) \ , \\
&L1_2 \text{:} -0.6411 \ (+1.1958) \ , \\
&DO_{22} \text{:} -0.6623 \ (-1.2169) \ .
\end{aligned}
\qquad (4.24)
$$

We see at $x = \frac{1}{2}$ the structure "40" has the lowest Madelung ordering energy in this group, whereas at $x = \frac{1}{4}$ or $x = \frac{3}{4}$, the DO_{22} structure has a lower Madelung ordering energy than the $L1_2$ structure.[79(b)] It is important to emphasize that for systems with significantly different A versus B bonding properties one can expect also significant charge transfer (proportional to λ), and that in such cases the SCPA introduces large errors in the ordering energy as seen in Eq. (4.24). This could alter qualitatively ordering predictions by the SCPA.

Having established the adequacy of our canonical set of figures (Fig. 2) and structures (Figs. 3 and 4) to cluster expansion of "simple" lattice properties, we proceed to apply this method to the total quantum mechanical energies.

V. CLUSTER EXPANSION OF EXCESS TOTAL ENERGIES

A. Electronic Hamiltonian and its solution

The excess total energy of Eq. (2.15), taken with respect to equivalent amounts of the solid binary constitutes in $A_{1-x}B_x$

$$\Delta E(s,V) = E(s,V) - (1-x_s)E(A,V_A)$$
$$- x_s E(B,V_B) \qquad (5.1)$$

was calculated for 12 fcc and (for AlNi and CuPd) 12 bcc structures $\{s\}$ shown in Figs. 3 and 4, respectively. The values of $\Delta E(s, V)$ at the equilibrium volume $V_{eq}(s)$ give the formation enthalpies $\Delta H(s)$. Note that the scale of $\Delta E(s, V)$ is not that of the total energy of a given structure, or that of the cohesive energy, but rather the *relative* energy of $A_n B_m$ with respect to its constituents ($\sim 10^{-2}$ eV). The large constant terms appearing in $E(s)$ (e.g., sum of atomic energies) are largely canceled in the construct of Eq. (5.1). We calculate $\Delta E(s, V)$ in the spin-unpolarized local-density approximation (LDA).[80] The LDA equations are solved by the linearized augmented-plane-wave (LAPW) method;[81] in one case (AlNi) we also use the LMTO method.[78] In the LAPW calculations we use the Wigner form[82] of ε_{xc} and V_{xc}, whereas in the LMTO calculation the form of von Barth and Hedin[83(a)] has been used (with the parameters given by Moruzzi et al.[83(b)]). The charge density was determined self-consistently and variationally from the semirelativistic (i.e., retaining all relativistic terms but spin-orbit interactions) local-density Hamiltonian.

Note that unlike some other calculations[48−50,52−57] (but not Ref. 51) of alloy energies our total energy expression includes the correct "double counting terms." Note further that all lattice sums over the potentially long-range interactions are calculated to convergence. Hence, the effective interaction energies p_F obtained from a superposition of such *total* energies [e.g., Eq. (4.2)] converge faster with the range of the figure F than would be expected had p_F been an interatomic interaction *potential*.

In the LAPW calculations of the total energies of the Cu-based intermetallic systems, we use the muffin-tin (MT) radii $R_{MT} = 2.4$ a.u for Au, Pd, Pt, and Rh, while for Cu we use $R_{MT} = 2.2$ a.u. No shape approximation is made for either the potential or the charge density. Inside the MT spheres, the nonspherical charge density and potential are expanded in terms of lattice harmonics of angular momentum $l \leq 8$. A basis set of about ~ 90 LAPW's/atom are used (equivalent to kineic energy cutoff of 16.7 Ry). The Brillouin-zone (BZ) integration is performed using the special-k point methods,[83(c)] with 60–400 special k points in an irreducible wedge of the BZ (depending on the structure and the material). The convergence error for total energy is estimated to be about 10 meV/atom.

The convergence of formation enthalpies with respect to the k-points sampling deserves further comments. We find that structures with 2–3 atoms per cell and small number of symmetry operations (e.g., the $L1_0$ and $L1_1$ structures) tends to require a large number of k points for obtaining converged results. For example, in the case of the CuPt alloy, the formation enthalpies of the unrelaxed $L1_1$ structure are -90.4, -107.6, and -111.9 meV/atom, using 60, 110, and 408 k points, respectively. Similarly for the unrelaxed $L1_1$ structure of the CuPd alloy, the enthalpies are -50.0 -55.8, -72.4 and -66.8 meV/atom, using 60, 110, 280, and 408 k points, respectively. On the other hand, the energies for other structures (e.g., fcc, bcc, $B2$, $L1_2$, and DO_{22}) converge rather rapidly with the number of k points. Using again the

$Cu_{1-x}Pt_x$ as an example, in the case of the $L1_2$ structure, the enthalpies for Cu_3Pt are -112.9 -116.4, and -115.8 meV/atom, using 20, 56, and 120 k points, respectively, while for $CuPt_3$ the enthalpies are -100.4 -96.4, and -96.3 meV/atom, using 20, 56, and 120 k points, respectively.

In the LMTO calculations we use the atomic-sphere approximation[78] (ASA) with the "combined correction"[84] (CC) (without the combined corrections, the integrals entering the Hamiltonian and overlap matrices are approximated by integrals over the Wigner-Seitz spheres. When the combined correction is included, a more realistic potential is used to treat the interstitials and sphere overlap region, and the integrals are evaluated over the correct Wigner-Seitz cell). The basis set consists of $l = 0$, 1, and 2 orbitals for both Ni and Al; the Wigner-Seitz spheres have the same sizes for both elements. 120 k points are used in the irreducible section of the Brillouin zone for pure Ni and Al (fcc or bcc), whereas for the cubic $A_n B_n$ compounds we use $120/(n + m)$ k points. For systems with lower symmetries the number of k points was increased in order to keep the spacing of points in the Brillouin zone nearly constant. The equilibrium lattice constant $a_{eq}(s)$ was found from a three-point parabolic fit to $E(a_i)$ $i = 1, 2, 3$; the energy was then recalculated at this interpolated $a_{eq}(s)$. The internal precision, is estimated at 10 meV/atom.

In both LMTO and LAPW calculations we have fit the equation of state $\Delta E(s, V)$ to a Murnaghan form[85]

$$\Delta E(s, V) = A(s) + C(s)V + D(s)V^{1-B'} , \qquad (5.2)$$

where B' is the pressure derivative of the bulk modulus.

B. Results for elemental solids and ordered compounds

Table IX gives the calculated equilibrium parameters for the elemental metals studied here. Our previous studies[27] [as well as the volume cluster expansion of Eq. (4.9)]

TABLE IX. Calculated [using a fit to Eq. (5.2)] and experimental equilibrium lattice constants a, bulk moduli B, and their pressure derivatives B' for solid Al, Ni, Cu, Rh, Pd, Pt, and Au.

Elemental Metal	a (Å)		B (GPa)		B'
	Calc.	Expt.[a]	Calc.	Expt.[b]	Calc.
Al(fcc)	3.994	4.050	87	72.2	
Al(bcc)	3.186		88		
Ni(fcc)	3.480	3.524	248	186	
Ni(bcc)	2.770		224		
Cu(fcc)	3.562	3.615	183.3	137	5.42
Cu(bcc)	2.836		179.2		5.67
Rh(fcc)	3.795	3.803	292.9	270.4	4.85
Pd(fcc)	3.882	3.890	211.1	180.8	5.28
Pd(bcc)	3.089		207.2		5.33
Pt(fcc)	3.935	3.923	287.0	278.3	5.28
Au(fcc)	4.094	4.078	182.5	173.2	5.60

[a]Reference 1.
[b]Reference 13(b).

suggested that little precision is lost for the Cu compounds if we linearize the equilibrium volumes and bulk moduli with respect to composition, i.e.,

$$V(s) = (1 - x_s)V(A) + x_s(B), \quad (5.3)$$

and similarly for $B(s)$. For example, the LAPW calculated volumes, bulk moduli B, and their pressure derivatives B' for the bcc elemental solids are

$$V(\text{Cu}) = 76.882 \text{ a.u.}^3,$$

$$B(\text{Cu}) = 1.798 \text{ Mbar} \quad B'(\text{Cu}) = 5.86,$$

$$V(\text{Pd}) = 99.454 \text{ a.u.}^3,$$

$$B(\text{Pd}) = 2.072 \text{ Mbar}, \quad B'(\text{Pd}) = 5.33.$$ (5.4)

The 50%-50% linear averages of the above are

$$\bar{V}(\text{CuPd}) = 88.168 \text{ a.u.}^3,$$

$$\bar{B}(\text{CuPd}) = 1.935 \text{ Mbar}, \quad (5.5)$$

$$\bar{B}'(\text{CuPd}) = 5.60,$$

whereas the directly calculated values for the CsCl structure of (CuPd) are

$$V(\text{CuPd}) = 87.744 \text{ a.u.}^3,$$

$$B(\text{CuPd}) = 1.952 \text{ Mbar}, \quad (5.6)$$

$$B'(\text{CuPd}) = 5.62,$$

i.e., the averages are within better than 1% from the directly calculated values. Results in the same range are obtained for Cu_3Pt and $CuPt_3$ in the $L1_2$ structure. We hence use the linearized volumes and bulk moduli for the

TABLE X. Formation enthalpies ΔH (in meV/atom) of the unrelaxed (ur) and relaxed (r) fcc compounds considered here, and the unit cell volumes (in cm^3/mole) at which the calculations were performed. The first line gives the unit cell volume, the second line gives the unrelaxed ΔH_{ur}, and the third line gives the relaxed ΔH_r. All Cu-based compounds are calculated using the LAPW method with the Wigner exchange correlation, whereas the Al-Ni compounds were calculated using the LMTO method with the von Barth-Hedin exchange correlation. The LMTO calculations were performed only for unrelaxed structure. Where available, we also give the formation enthalpies obtained by previous calculations and experimental values.

	$L1_2$ A_3B	DO_{22} A_3B	$\beta1$ A_2B	$L1_0$ AB	$L1_1$ AB	"40" A_2B_2	$Z2$ A_2B_2	$\beta2$ AB_2	DO_{22} AB_3	$L1_2$ AB_3
	7.685	7.685	7.979	8.567	8.567	8.567	8.567	9.155	9.450	9.450
$A = $Cu	−35.1	−30.8	59.9	−33.4	68.1	−15.2	155.3	46.4	−9.1	−16.1
$B = $Au	−35.1	−31.7	−5.6	−62.0	28.6	−20.0	−16.9	−49.9	−10.8	−16.1
	−37[a]									
	−74.2[b]			−91.1[b]						−59.4[b]
	−64.9[c]			−69.7[c]						−34.0[c]
	7.304	7.304	7.471	7.805	7.805	7.805	7.805	8.139	8.307	8.307
$A = $Cu	−85.0	−75.5	−36.4	−75.9	−66.8	−76.4	−4.3	−48.6	−46.4	−53.4
$B = $Pd	−85.0	−76.4	−45.6	−86.3	−82.0	−84.6	−72.0	−72.0	−46.4	−53.4
	−78[d]			−68[d]						−49[d]
	7.395	7.395	7.592	7.988	7.988	7.988	7.988	8.383	8.580	8.580
$A = $Cu	−115.8	−96.7	−40.8	−83.3	−111.9	−63.8	34.7	−31.2	−65.9	−96.3
$B = $Pt	−115.8	−97.6	−66.4	−98.9	−128.9	−63.8	−43.0	−79.0	−65.9	−96.3
	−117[d]			−117.0[d]	−206.7[d]					−136[d]
					−174.3[b]					
	7.159	7.159	7.277	7.515	7.515	7.515	7.515	7.753	7.872	7.872
$A = $Cu	68.5	72.0	110.2	168.8	98.9	94.6	78.5	100.8	57.7	128.4
$B = $Rh	68.5	72.0	108.0	164.0	92.8	93.7	75.9	100.8	57.7	128.4
	8.258	8.285	7.891	7.191	7.337	7.173	7.479	6.861	6.675	6.630
$A = $Al	−233	−237	−234	−580	−355	−594	−110	−351	−476	−504
$B = $Ni	−220[e]			−600[e]						−450[e]
									−438[f]	−486[f]
										−425[g]

[a]Calculated results of Ref. 86 at the experimental lattice constant, using the linear augmented Slater-type-orbital method and the Hedin-Lundqvist exchange-correlation.
[b]Experimental results of Ref. 5.
[c]Calculated results for the unrelaxed structures of Ref. 62(a) using the augmented spherical-spherical wave (ASW) method and the von Barth-Hedin exchange correlation.
[d]Calculated results for the unrelaxed structures of Ref. 62(b) using the ASW method and the von Barth-Hedin exchange correlation.
[e]Calculated results of Ref. 87 using the ASW method and the von Barth-Hedin exchange correlation.
[f]Calculated results of Ref. 88 using the LMTO method and the Hedin-Lundqvist exxhange correlation
[g]Experimental result of Ref. 7(b).

Cu compounds [this constitutes a significant computational economy as we only need to calculate $\Delta E(s, V)$ at a single volume]. Since the variations are somewhat larger for AlNi [in particular, $V_{eq}(x)$ of two structures of the same composition are slightly different], we do not linearize V and B for these compounds. Since the pressure derivative B' contains a significant numerical uncertainty (being a third derivative), we have not attempted to calculate it for each structure; instead, we use it as an adjustable parameter in the fit of Eq. (4.3). This gives for the fcc structures.

$$B' \text{ (CuAu)} = 1.5, \quad B'(\text{AlNi}) = 5.1 \ . \tag{5.7}$$

For all other compounds we used the harmonic value $B' = -1$, which is very close to the minimum of the variance [Eq. (4.3)]; the latter is found to be rather insensitive to the value of B' near -1. Tables X and XI list our calculated formation enthalpies for all intermetallic compounds studied here. Where available we also give experimental values[5,7] and values from other calculations.[86–88]

In the relaxed LAPW calculations we have allowed the c/a ratio and the position of the atoms inside the unit cell (that are not fixed by symmetry) to vary so as to minimize $\Delta E(s, V)$ at V given by Eq. (5.3). When such structural degrees of freedom are unavailable (e.g., in $L1_2$), relaxation does not exist; otherwise, it lowers the energy. This lowering is enormous in structures possessing a number of such structural degrees of freedom (e.g., $\beta 1$, $\beta 2$, $Z2$), but is smaller in other structures (e.g., DO_{22}, "40").

Tables X and XI show that the augmented-spherical wave (ASW) method used in Refs. 62 and 87 produces significantly more negative unrelaxed formation enthalpies (relative to the more accurate LAPW method used here) for the fcc CuAu and CuPt, and bcc CuPd compounds, whereas the results for fcc CuPd are comparable to ours. The LMTO results of Ref. 88 for AlNi are similar to the present LMTO result, as are the ASW results[87] for this system.

C. Extracting effective cluster interaction energies

The cluster expansion of the excess total energy $\Delta E(s, V)$ of Eq. (2.16) reads

$$\Delta E(s, V) = \sum_{m > 0} \sum_{k > 1} [\overline{\Pi}_{k,m}(s) - \eta] D_{k,m} J_{k,m}(V) , \tag{5.8}$$

where $\{J_{k,m}(V)\}$ are the volume-dependent effective interaction energies and $\eta = 1$ for $k = $ even and $(2x_s - 1)$ for $k = $ odd. We have extracted $N_F = 8$ functions $\{J_{k,m}(V)\}$ from the $N_s = 12$ excess total energy functions $\{\Delta E(s, V)\}$ and the lattice-averaged spin products $\{\overline{\Pi}_{k,m}(s)\}$ (Tables III and IV) by minimizing the variance

$$\sum_{s}^{N_s} \omega_s \left[\Delta E(s, V) - \sum_{m > 0} \sum_{k > 1} [\overline{\Pi}_{k,m}(s) - \eta] D_{k,m} J_{k,m}(V) \right]^2 = \text{minimum} , \tag{5.9}$$

with the weights ω_s given by Eq. (4.4) and Table V. Tables XII and XIII compare the directly calculated (LAPW or LMTO) $\Delta E(s, V)$ for fcc and bcc structures, respectively, with those obtained from the cluster expansion (5.8), using the coefficients $J_{k,m}(V)$ determined from Eq. (5.9) [the comparison is given at the equilibrium volume obtained from Eq. (4.9)]. The cluster expansion was carried out separately for the "unrelaxed"

TABLE XI. Formation enthalpies ΔH (in meV/atom) of the unrelaxed (ur) and relaxed (r) bcc compounds considered here, and the unit cell volumes (in cm^3/mole) at which the calculation was performed. The first line gives the unit cell volume, the second line gives the unrelaxed ΔH_{ur}, and the third line gives the relaxed ΔH_r. All Cu-based compounds are calculated using the LAPW method with the Wigner exchange-correlation, whereas the Al-Ni compounds were calculated using the LMTO method with the von Barth-Hedin exchange correlation. The LMTO calculations were performed only for unrelaxed structure. Where available, we also give the formation enthalpies obtained by previous calculations and experimental values.

	DO_3 A_3B	$L6_0$ A_3B	$C11_b$ A_2B	$B2$ AB	A_1 AB	$B32$ A_2B_2	$B11$ A_2B_2	$C11_b$ AB_2	$L6_0$ AB_3	DO_3 AB_3
	7.364	7.364	7.537	7.868	7.868	7.868	7.868	8.206	8.372	8.372
$A =$ Cu	-37.7	-29.9	-50.8	-97.6	9.1	13.9	40.3	17.4	18.7	30.8
$B =$ Pd	-37.7			-97.6	-7.4	13.9	30.8			30.8
				-223^a						
				-142.3^b						
	8.307	8.269	7.811	7.079	7.310	7.270	7.395	6.810	6.667	6.678
$A =$ Al	-166	-175	-353	-787	-383	-449	-207	-504	-449	-490
$B =$ Ni				-741^c						

[a]Calculated results of the unrelaxed structures of Ref. 62(b) using ASW method and the von Barth-Hedin exchange correlation.
[b]Experimental result of Ref. 5 at $x = \frac{1}{2}$.
[c]Experimental result of Ref. 7(b).

TABLE XII. Comparison of the directly calculated (LAPW or LMTO) and the cluster-expanded [Eq. (5.8) using $N_F = 8$ and $N_s = 12$] unrelaxed excess total energies (in meV/atom) for the fcc-based intermetallic structures. The 12 structures are shown in Fig. 3; the interaction energies are depicted in Table I and Fig. 2(a). The last two lines show the standard deviation χ of the fit for both unrelaxed and relaxed structures. $B' = -1$, except for CuAu, for which $B' = 1.5$, and AlNi, for which $B' = 5.1$

fcc structure	$Cu_{1-x}Au_x$ LAPW	Fit	$Cu_{1-x}Pd_x$ LAPW	Fit	$Cu_{1-x}Pt_x$ LAPW	Fit	$Cu_{1-x}Rh_x$ LAPW	Fit	$Al_{1-x}Ni_x$ LMTO	Fit
A	0.0	0.0	0.0	0.0	0.0	0.0	0.0	0.0	0	0
$L1_2$ (A_3B)	−35.1	−37.9	−85.0	−79.3	−115.8	−112.5	68.5	99.3	−233	−236
DO_{22} (A_3B)	−30.8	−29.9	−75.5	−77.4	−96.7	−97.9	72.0	61.7	−237	−236
$\beta1$ (A_2B)	59.9	57.1	−36.4	−40.8	−40.8	−37.8	110.2	98.5	−234	−257
$L1_0$ (AB)	−33.4	−32.8	−75.9	−78.4	−83.3	−91.2	168.8	170.2	−580	−588
$L1_1$ (AB)	68.1	68.1	−66.8	−66.8	−111.9	−111.9	98.9	98.9	−355	−355
"40" (A_2B_2)	−15.2	−15.9	−76.4	−74.8	−63.8	−61.3	94.6	95.5	−594	−590
$Z2$ (A_2B_2)	155.3	154.6	−4.3	−3.6	34.7	31.7	78.5	81.9	−110	−109
$\beta2$ (AB_2)	46.4	50.8	−48.6	−46.0	−31.2	−27.2	100.8	106.1	−351	−355
DO_{22} (AB_3)	−9.1	−8.7	−46.4	−47.7	−65.9	−69.7	57.7	66.1	−476	−483
$L1_2$ (AB_3)	−16.1	−17.4	−53.4	−49.4	−96.3	−85.0	128.4	103.2	−504	−484
B	0.0	0.0	0.0	0.0	0.0	0.0	0.0	0.0	0	0
Deviation										
$\chi_{unrel.}$ (meV)		1.9		2.5		4.1		10.6		9.0
$\chi_{relaxed}$ (meV)		16.3		11.9		7.0		10.6		

geometries, i.e., when the total energies are varied with respect to the unit cell volumes but the A and B atoms are assumed to reside on their cubic fcc or bcc sites, and for the "relaxed" geometries, when the total energy is optimized with respect to all structural degrees of freedom consistent with the respective space group symmetry.

Table XII and XIII show that the cluster expansion (5.8) describes the excess energies of the unrelaxed ordered structure to within ~ 3 meV/atom for the fcc structures of CuAu, CuPd, and CuPt, while the error is ~ 10 meV/atom for fcc CuRh and AlNi and for the two

bcc structures. On the other hand we see from Table XII that when the ordered structures are allowed to relax, the truncated cluster expansion result in significantly larger errors (compare the standard deviations, χ_{unrel} and $\chi_{relaxed}$ in these tables). We next briefly discuss the role of relaxation.

D. Role of relaxation

The molar volumes and atomic positions in disordered alloys and ordered intermetallic compounds generally de-

TABLE XIII. Comparison of the directly calculated (LAPW or LMTO) and the cluster-expanded [Eq. (5.8), using $N_F = 8$ and $N_s = 12$] unrelaxed excess energies (in meV/atom) for the bcc-based structures. The 12 structures are depicted in Fig. 4 and the eight interactions are shown in Fig. 2(b). $B' = -1.0$ for both CuPd and AlNi. We also give the standard deviation χ.

bcc structure	$Cu_{1-x}Pd_x$ LAPW	Fit	$Al_{1-x}Ni_x$ LMTO	Fit
A	41.2	41.2	55	55
DO_3 (A_3B)	−37.7	−44.7	−166	−143
$L6_0$ (A_3B)	−29.9	−34.3	−175	−201
$C11_b$ (A_2B)	−50.8	−36.2	−353	−337
$B2$ (AB)	−97.6	−93.8	−787	−773
A_1 (AB)	9.1	9.3	−383	−363
$B32$ (A_2B_2)	13.9	13.7	−449	−469
$B11$ (A_2B_2)	40.3	41.5	−207	−213
$C11_b$ (AB_2)	17.4	0.5	−504	−511
$L6_0$ (AB_3)	18.7	22.5	−449	−458
DO_3 (AB_3)	30.8	38.5	−490	−470
B	58.6	58.6	30	30
Deviation				
χ_{unrel} (meV)		8.1		16.5

viate from what simple rules might suggest (e.g., Zen's rule for molar volumes or ideal fcc positions for atomic coordinates); we refer collectively to these deviations as "relaxation." We will distinguish "volume relaxation" (when molar volumes are nonideal) from "sublattice relaxations" (when atoms do not reside on ideal fcc sites). Carlsson[63(c)] distinguished three levels of approximation for "volume relaxation" in the context of the method of "superposition of periodic structures" [Eqs. (4.1)–(4.6)]. These are distinguished by the form of the molar volume used to evaluate the excess energy $P(s, V) = \Delta E(s, V)$ of ordered structures in Eq. (4.1).

(i) Complete neglect of volume relaxation. This corresponds to the use of a single (composition-independent) arbitrary volume V_0 in the excess energy $P(s) = \Delta E(s, V)$ of Eq. (4.2) for *all* ordered structures s. This was deemed unphysical.[63(c)]

(ii) "Global relaxation," i.e., when $\Delta E(s, V)$ represents an equation of state calculated continuously as a function of V. In this case the interaction energies of Eq. (4.2) are volume dependent. The equilbrium volume is calculated variationally [Eq. (4.10)] or simplifed further [Eq. (5.9)]. Our cluster expansions shown in Tables XII and XIII correspond to this model.

(iii) "Local relaxation," i.e., when $\Delta E(s, V)$ is calculated for each structure s at a single volume V_s that minimizes $\Delta E(s, V)$. In this case $\Delta E(s, V_s) \equiv \Delta H_s$ is the formation enthalpy of compound s. We find that this procedure leads to a very slow convergence of the cluster expansion: e.g., for CuAu the standard deviation increases to 16.3 meV from 1.9 meV, while for fcc CuPd it is 11.9 meV rather than 2.5 meV. Hence, introduction of a continuous volume variable in Eq. (5.14) considerably improves the convergence of the series. We will, hence, not consider local relaxation in what follows.

Another form of volume relaxation was recently considered by Sluiter *et al.*[63(d)]: the excess energy $\Delta E(s, V)$ of the unrelaxed (ur) lattice was decomposed into a "chemical" and "elastic" pieces as

$$\Delta E_{ur}(s, V) = \Delta E_{chem}(s, V) + \Delta E_{elast}(x_s, V) , \qquad (5.10)$$

where the elastic energy is given by

$$\Delta E_{elast}(x, V) = Q(x)[V - (1-x)V_A - xV_B]^2 . \qquad (5.11)$$

Here ΔE_{ur} refers to the excess energy calculated with LAPW as a function of volume, assuming that the atoms reside on ideal fcc sites, V_A and V_B are the equilibrium volumes of pure A and B, respectively, and $Q(x)$ is a function of composition calculated from harmonic elasticity. The cluster expansion of Eq. (4.1) was performed with

$$P(s, V) = \Delta E_{chem}(s, V)$$

$$= \Delta E_{ur}(s, V) - \Delta E_{elast}(x_s, V) \qquad (5.12)$$

alone; the resulting chemical interaction energies $\{p_F\}$ were then used to construct the chemical energy of arbitrary configurations, to which the elastic energy of Eq. (5.11) was then added. Note, however, that for *ordered* structures $\Delta E_{chem}(s, V) + \Delta E_{elast}(x_s, V)$ of Eqs. (5.11) and (5.12) produce the total energy $\Delta E_{ur}(s, V)$ of a lattice in which the atomic positions are unrelaxed; our Table X shows that this misses considerable energies (compare the second and third lines in this table, giving ΔE_{ur} and ΔE_R, respectively). Note further that to the extent that equilibrium molar volume $V(x)$ of the alloy is linear with composition and the bulk moduli difference $\Delta B = B_B - B_A$ is small $\Delta E_{chem}(s, V) \approx \Delta E_{chem}[s, V(x_s)] \equiv \Delta H_s$, hence, this model[63(d)] will give results similar to that of the "local relaxation" model[63(c)] and lead to a slow convergence of the cluster expansion.

We conclude that "global volume relaxation" is a consistent model for describing alloy-induced changes in V, but that *"sublattice relaxation"* needs, in general, to be added. The basic reason that "global volume relaxation" plus "sublattice relaxation" (reflected in the relaxation energies of Tables X and XI) lead to a slowly convergent cluster expansion (Tables XII and XIII) can be appreciated as follows: when all atoms are assumed to reside on ideal fcc sites, the figures (k,m) exhibit symmetry properties [Eqs. (2.6)–(2.8)] that lead to certain degeneracies [expressed by the factor D_F in (2.11)]. In this case, $J_F = J_f$ and the cluster expansion may be carried out only on prototype (symmetry-unique) figures F. In the presence of sublattice relaxation, however, part of this degeneracy is removed, e.g., the pair figure (2,1) along the [001] relaxation direction of the A_2B_2 [001] superlattice (Z2) is no longer symmetry related to this figure in the perpendicular direction. Hence, since relaxation can alter the size of the symmetry-related figures (which have the same size and associated energy in the unrelaxed lattice), truncation of Eq. (2.5) for *relaxed* configurations could make J_F very different from J_f, leading to a slower convergence of Eq. (2.9) for the same number of figures. To quantify this, consider a simple numerical example. The "Z2" structure, consisting of a Cu_2Au_2 superlattice along the [001] direction (Fig. 3) relaxes such that the tetragonal $\eta \equiv c/a$ ratio becomes 0.825 in the Cu segment and 1.175 in the Au segment. In the "ideal" structure, $c/a = 1$ in both segments. The relaxation energy given in Table X then corresponds to

$$\Delta E(Z2, \eta_{Cu} = 0.825, \eta_{Au} = 1.175) - \Delta E(Z2, \eta_{Cu} = 1, \eta_{Au} = 1) = -139 \text{ meV/atom} . \qquad (5.13)$$

To see what fraction of this relaxation energy results from elastic effects, we will model it from the deformation energies of the *constituent* solids (i.e., charge transfer is excluded). The sum of the deformation energies of the constituents is

$$\Delta E_{Rel}(s, x_s) = \{E[Cu, \eta = 0.825] - E[Cu, \eta = 1]\}$$

$$+ \{E[Au, \eta = 1.175] - E[Au, \eta = 1]\}$$

$$= -153 \text{ meV/atom} . \qquad (5.14)$$

LU, WEI, ZUNGER, FROTA-PESSOA, AND FERREIRA

44

We see that the sublattice relaxation of the constituents [Eq. (5.14)] accounts for most of the total sublattice relaxation energy [Eq. (5.13)]. Clearly, this type of relaxation is missed by the models of Carlsson[63(a)] or Sluiter et al.[63(d)] [Eqs. (5.10)–(5.12)].

This discussion suggests that sublattice relaxation is likely to be less of a problem in describing *disordered* phases, since there one uses a *configuration average* over the energies J_F, hence, much of the symmetry lowering will be averaged out. Fortunately, this can be tested, as follows.

E. Predicting structural energies from the cluster expansion

To examine the transferability of the interaction energies $\{J_{k,m}(V)\}$, we have recalculated them from Eq. (5.9) for $N_F = 8$ figures, *using, however, a set of only $N_s = 10$ out of 12 structures.* The resulting interaction energies are then used in Eq. (5.8) to predict the excess energies of the two *remaining* structures, not used in determining the J's. Comparison of these predicted energies with those calculated directly by the LAPW or the LMTO gives this "prediction error" shown in Table XIV for five pairs of structures for each compound. We see that the standard deviation χ over these five predicted energy pairs is within the underlying precision of the direct, LAPW or

LMTO calculations, except for $Cu_{1-x}Pt_x$ ($\chi = 13.4$ meV) and $Al_{1-x}Ni_x$ ($\chi = 22.1$ meV) (in the latter case, the error is still much smaller than ΔH itself).

We have also calculated the excess enthalpy of the random alloy using different sets of J's obtained from the various combinations of 10 structures. Table XIV exhibits robust predictions of these excess enthalpies (given at $x = \frac{1}{2}$) *both for the relaxed and for the unrelaxed structures.* We conclude that the interaction energies $\{J_F\}$ extracted from the *relaxed* equations of state $\Delta E_R(s, V)$ provide an adequately converged description of the *disordered* phase. In what follows we will use this description. However, *for ordered* phases we will use this unrelaxed J_F; we will comment on this below only to the extent that the use of relaxed J_F leads to qualitatively different conclusion (see Sec. VI B 3 below). Development of a comprehensive treatment of volume and sublattice relaxation on equal footings is clearly lacking and needed.

F. Magnitude and range of the interaction energies $J_{k,m}(V)$

The unrelaxed interaction energies $J_{k,m}[V(x)]$ are depicted in Fig. 5 for fcc $Cu_{1-x}Au_x$, $Cu_{1-x}Pt_x$, and $Cu_{1-x}Rh_x$, while Figs 6 and 7 give the interaction energies for $Cu_{1-x}Pd_x$ and $Al_{1-x}Ni_x$, respectively, both for the fcc and the bcc cases. Note the following features: (i) In all cases but $Cu_{1-x}Rh_x$, the energy expansions con-

TABLE XIV. First-principles excess energies $\{\Delta E(s,V)\}$ are available for the 12 fcc-based structures: A, B, $L1_0$, "40", $L1_1$, $Z2$, $L1_2$, DO_{22}, and β shown in Fig. 3. Using 10 out of these 12 structures we cluster expand their energies according to Eq. (5.8) thus determining the 8 interaction parameters of Fig. 2(a). Using these we then predict the formation enthalpies $\Delta H(s)$ for the two remaining structures not used in the fit. This table compares the predicted enthalpy with the "exact" value (in parentheses) for five different pairs of structures not included in the fit; χ gives the deviation in meV. We also give the predicted energies of the random alloy at $x = \frac{1}{2}$ for both unrelaxed (ur) and relaxed (r) systems: (Unit: meV/atom.) While the precision is lower than that obtained using the 12 structures in fit (Tables XII), the prediction error is still remarkably small on the scale of the LAPW error (~ 10 meV/atom).

Struct. not in fit	ΔH first struct.	$Cu_{1-x}Au_x$ ΔH second struct.	ΔH random ur	ΔH random r	ΔH first struct.	$Cu_{1-x}Pt_x$ ΔH second struct.	ΔH random ur	ΔH random r
$\beta1,\beta2$	57.1(59.9)	52.1(46.4)	68.5	−6.0	−35.6(−40.8)	−23.9(−31.2)	−45.6	−78.3
$L1_2,L1_0$	−38.1(−35.1)	−33.6(−32.8)	68.3	−8.8	−120.2(−115.8)	−112.9(−83.8)	−43.6	−77.6
$L1_2,L1_2$	−39.7(−35.1)	−18.9(−16.1)	68.4	1.0	−108.0(−115.8)	−78.0(−96.3)	−47.1	−76.4
DO_{22},DO_{22}	−26.3(−30.8)	−6.2(−9.1)	68.5	2.6	−104.6(−96.7)	−84.2(−65.9)	−50.4	−78.9
$DO_{22},\beta1$	−26.4(−30.8)	56.8(59.9)	69.1	−1.9	−102.3(−96.7)	−36.7(−40.8)	−47.0	−77.8
χ		3.7	0.3	4.3		13.4	2.2	0.8

| Struct. not in fit	ΔH first struct.	$Cu_{1-x}Pd_x$ ΔH second struct.	ΔH random ur	ΔH random r	ΔH first struct.	$Al_{1-x}Ni_x$ ΔH second struct.	ΔH random ur	ΔH random r
$\beta1,\beta2$	−41.2(−36.4)	−46.9(−48.6)	−47.8	−78.5	−259(−234)	−351(−351)	−329	
$L1_2,L1_0$	−78.6(−85.0)	−80.6(−75.9)	−47.2	−79.2	−250(−233)	−611(−580)	−326	
$L1_2,L1_2$	−75.4(−85.0)	−45.9(−53.4)	−47.9	−73.5	−231(−233)	−472(−504)	−329	
DO_{22},DO_{22}	−85.1(−75.5)	−53.9(−46.4)	−50.1	−77.3	−239(−237)	−507(−476)	−335	
$DO_{22},\beta1$	−83.6(−75.5)	−41.9(−36.4)	−49.2	−77.4	−228(−237)	−265(−234)	−330	
χ		7.2	1.1	2.0		22.1	2.8	
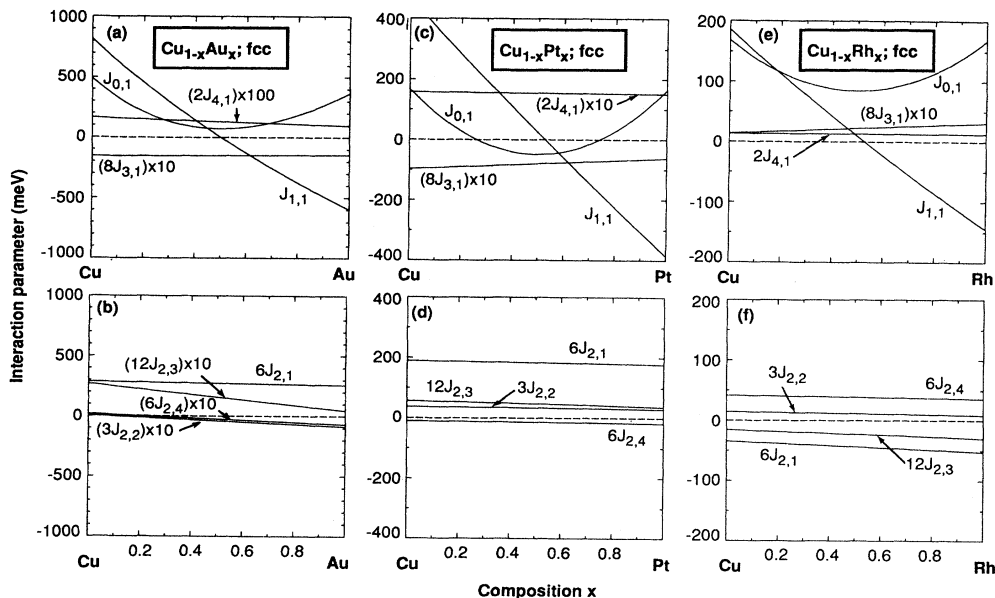
FIG. 5. Fcc interaction energies $J_{k,m}[V(x)]$ obtained from the cluster expansion for (a) and (b) $Cu_{1-x}Au_x$, (c) and (d) $Cu_{1-x}Pt_x$, (e) and (f) $Cu_{1-x}Rh_x$.

verge with respect to the figure sizes in the sense that among pair interactions the nearest-neighbor terms $D_{2,1}J_{2,1}$ are considerably larger than the longer-range pair interactions, and the three- and four-body terms are rather small. This is illustrated in Fig. 8 for $x=\frac{1}{2}$. (ii) The magnitude of the pair interactions $J_{2,m}(V)$ do not decay monotonically with the interatomic separation m;

the fourth-neighbor pair interaction $J_{2,4}$ is often larger than the third-neighbor pair interaction $J_{2,3}$. A similar trend has been observed in tight-binding calculations for transition metal alloys.[53] (iii) The dominant nearest-neighbor pair interaction $J_{2,1}$ is "antiferromagnetic" $(J_{2,1}>0)$ in the compound-forming alloys $Cu_{1-x}Au_x$, $Cu_{1-x}Pt_x$, $Cu_{1-x}Pd_x$, and $Al_{1-x}Ni_x$, while for the
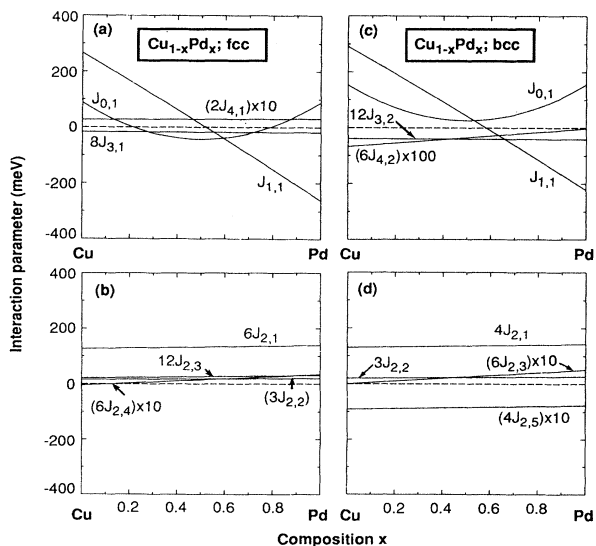
FIG. 6. Interaction energies $J_{k,m}[V(x)]$ obtained from the cluster expansion, comparing fcc $Cu_{1-x}Pd_x$ [parts (a) and (b)] with bcc $Cu_{1-x}Pd_x$ [parts (c) and (d)].
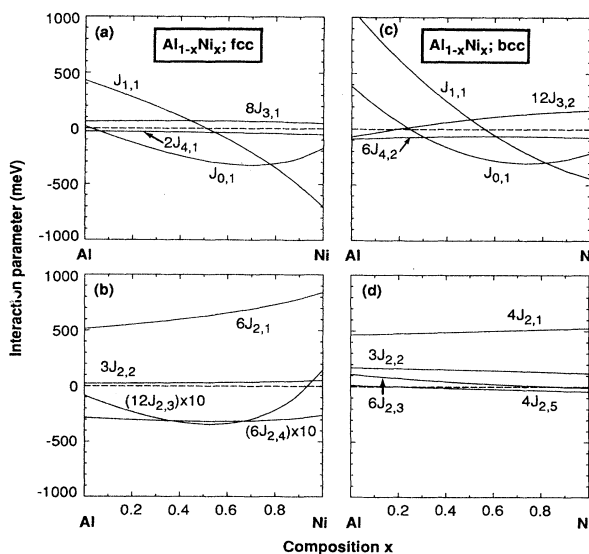
FIG. 7. Interaction energies $J_{k,m}[V(x)]$ obtained from the cluster expansion, comparing fcc $Al_{1-x}Ni_x$ [parts (a) and (b)] with bcc $Al_{1-x}Ni_x$ [parts (c) and (d)].
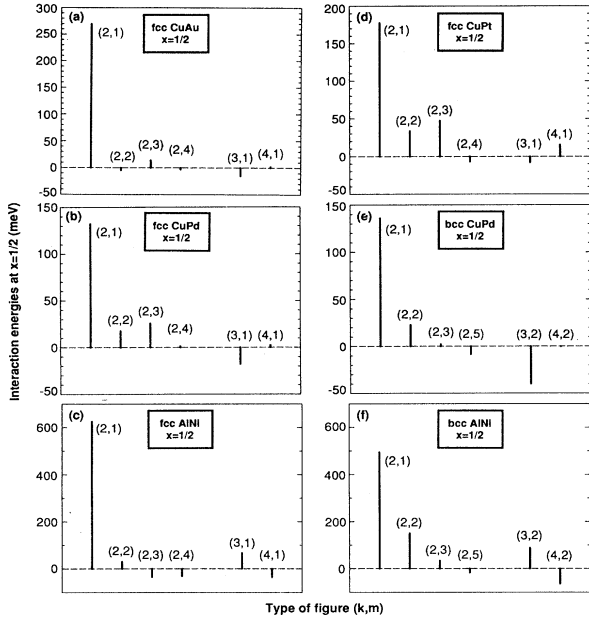
FIG. 8. Interaction energies $J_{k,m}[V(x)]$ at $x = \frac{1}{2}$, showing they decay with the order (k) and size (m) of each figure.

known[4−7] phase-separating $Cu_{1-x}Rh_x$ case, it is "ferromagnetic" $(J_{2,1} < 0)$. Concomitantly, $J_{0,1}(x = \frac{1}{2})$ [which, by Eq. (2.18) gives the excess enthalpy of the ranom alloy at $x = \frac{1}{2}$] is negative for all compound-forming systems, and positive for the phase-separating $Cu_{1-x}Rh_x$ system. (iv) The excess enthalpy of the ran-

dom alloy $J_{0,1}(x = \frac{1}{2})$ could change sign as the Bravais lattice is changed, e.g., it is negative (stable) in fcc $Cu_{0.5}Pd_{0.5}$, but positive (unstable) in bcc $Cu_{0.5}Pd_{0.5}$. Hence, despite the fact that $Cu_{0.5}Pd_{0.5}$ orders in a bcc structure (see Fig. 1 and Fig. 9 below), when disordered, it is stabler in the fcc structure, as observed experimentally.[3−6] (v) The second-neighbor pair interaction $J_{2,2}$ is uniquely negative ("ferromagnetic") for CuAu (Fig. 8) while $J_{2,1}$ is positive ("antiferromagnetic"), indicating that this alloy is frustrated.

Numerous previous applications[61−68] have restricted energies $\{J_{k,m}(V)\}$ to just first fcc neighbors ($m = 1$); the five $\{J_{k,1}(V)\}$ values for $k = 0, 1, 2, 3,$ and 4 were determined by direct inversion of Eq. (4.2) using five values of $\Delta E(s, V)$. Table XV applies this Connolly-Williams[61] procedure to the alloys studied here. The quality of the fit is rather poor (compare with Table XII that uses a converged set of interactions). Furthermore, this approach spuriously produces a degeneracy in the energies of certain structure pair, e.g., $\{L1_2; DO_{22}\}$ and $\{L1_0; "40"\}$, and misses the fact that $L1_1$ structure is the lowest energy for CuPt at $x = \frac{1}{2}$. Clearly, the cluster expansion needs to be extended (Tables XII and XIII) above this nearest-neighbor model.

VI. GROUND STATES

A. Finding the ground-state line

As discussed in the Introduction, our aim, is to identify among 2^N possible lattice configurations, those that are ground state, using a input first-principle total energy calculation on only $O(10)$ structures. The preceding section

TABLE XV. Comparison of the directly calculated (LAPW or LMTO) and the cluster-expanded [Eqs. (4.1) and (4.2), using the $N_F = N_s = 5$ Connolly and Williams structures] unrelaxed excess total energies (in meV/atom) for the fcc-based intermetallic structures. The last line shows the standard deviation χ of the fit for the unrelaxed. $B' = -1$, except for CuAu, for which $B' = 1.5$, and AlNi, for which $B' = 5.28$. Note that the use of just first-neighbor interactions ($J_{0,1}$, $J_{1,1}$, $J_{2,1}$, $J_{3,1}$, and $J_{4,1}$) leads to significant errors, except for the five structures A, $A_3B(L1_2)$, $AB(L1_0)$, $AB_3(L1_2)$, and B used in the fit. This approach also produces a spurious degeneracy between $\{L1_2, DO_{22}\}$ and $\{L1_0, "40"\}$.

| fcc | $Cu_{1-x}Au_x$ | | $Cu_{1-x}Pd_x$ | | $Cu_{1-x}Pt_x$ | | $Cu_{1-x}Rh_x$ | | $Al_{1-x}Ni_x$ | |
structure	LAPW	Fit	LAPW	Fit	LAPW	Fit	LAPW	Fit	LMTO	Fit
A	0.0	0.0	0.0	0.0	0.0	0.0	0.0	0.0	0	0
$L1_2$ (A_3B)	−35.1	−35.1	−85.0	−85.0	−115.8	−115.8	68.5	68.5	−233	−233
DO_{22} (A_3B)	−30.8	−35.1	−75.5	−85.0	−96.7	−115.8	72.0	68.5	−237	−233
$\beta1$ (A_2B)	59.9	61.2	−36.4	−20.0	−40.8	−10.6	110.2	129.2	−234	−283
$L1_0$ (AB)	−33.4	−33.4	−75.9	−75.9	−83.3	−83.3	168.8	168.8	−580	−580
$L1_1$ (AB)	68.1	60.0	−66.8	−36.2	−111.9	−52.6	98.9	119.3	−355	−296
"40" (A_2B_2)	−15.2	−33.4	−76.4	−75.9	−63.8	−83.3	94.6	168.8	−594	−580
$Z2$ (A_2B_2)	155.3	156.0	−4.3	28.4	34.7	64.3	78.5	125.6	−110	−146
$\beta2$ (AB_2)	46.4	48.5	−48.6	−22.3	−31.2	−5.9	100.8	132.6	−351	−361
DO_{22} (AB_3)	−9.1	−16.1	−46.4	−53.4	−65.9	−96.3	57.7	128.4	−476	−504
$L1_2$ (AB_3)	−16.1	−16.1	−53.4	−53.4	−96.3	−96.3	128.4	128.4	−504	−504
B	0.0	0.0	0.0	0.0	0.0	0.0	0.0	0.0	0	0
Deviation										
χ_{unrel} (meV)		7.7		18.5		28.4		43.3		29.4

demonstrated that a converged Ising representation of the quantum-mechanically calculated excess total energy can indeed be obtained from such a limited information. We now turn to the question of identification of ground-state structures from such an Ising representation. To define what is meant by a ground state, consider the three configurations σ, α, and β with concentration of B atoms $x(\sigma)$, $x(\alpha)$, and $x(\beta)$ in the order

$$x(\alpha) \leq x(\sigma) \leq x(\beta) . \tag{6.1}$$

If the energy $E(\sigma)$ is larger than the linear average of $E(\alpha)$ and $E(\beta)$, i.e., if

$$E(\sigma) > \frac{x(\sigma) - x(\beta)}{x(\alpha) - x(\beta)} E(\alpha) + \frac{x(\sigma) - x(\alpha)}{x(\beta) - x(\alpha)} E(\beta) \tag{6.2}$$

then configuration σ *does not belong to the ground state* because a mixture of the phases α and β would have a lower energy. On the other hand, if no pair of configuration (α, β) satisfy Eqs. (6.1) and (6.2), then σ does belong to the ground state. A plot of the ground-state energy as a function of the concentration x consists then of straight line pieces between "breaking points" that correspond to the ground-state ordered (periodic) configurations of atoms. Any configuration σ could be represented in such a plot by a point $\{x(\sigma), E(\sigma)\}$. This point would be *above* the ground-state line (GSL) if Eqs. (6.1) and (6.2) are satisfied for a certain pair α and β.

The ground state of a Hamiltonian of the type given in Eq. (2.4) is a classical problem in magnetism and in theory of the alloys.[18-24] For fcc alloys, the most complete search for the ground state was given by Kanamori and Kakehashi[19] (KK) while for bcc it was given by Finel and Ducastelle.[20]

Kanamori and Kakehashi[19] studied the exact ground state in fcc symmetry, assuming: (i) *volume and concentration independent interactions* (denoted here $v_{k,m}$), (ii) null triangle $(k,m) = (3,1)$ and tetrahedron $(k,m) = (4,1)$ interactions, i.e.,

$$v_{3,1} = v_{4,1} = 0 , \tag{6.3}$$

and (iii) that the first-neighbor pair interaction is much larger than the other interactions, i.e.,

$$|v_{2,1}| \gg |v_{2,2}| ; |v_{2,3}| ; |v_{2,4}| . \tag{6.4}$$

Under assumption (i) one can use Eqs. (2.13) and (2.14) to obtain the sum rules

$$\begin{aligned} v_{0,1} &= -\sum_k^{\text{even}} \sum_m D_{k,m} v_{k,m} , \\ v_{1,1} &= -\sum_k^{\text{odd}} \sum_m D_{k,m} v_{k,m} . \end{aligned} \tag{6.5}$$

The problem is then reduced to three parameters $v_{2,2}$, $v_{2,3}$, and $v_{2,4}$, or two ratios $v_{2,2}/v_{2,4}$ and $v_{2,3}/v_{2,4}$. Kanamori and Kakehashi[19] mapped all fcc ground states containing ≤ 16 atoms/cell as a function of these two ratios, using assumptions (i)–(iii).

Although illuminating, the Kanamori and Kakehashi[19] assumptions are seldom met in practical cases. For instance, we find that in most cases the interaction energies depend on volume and composition (Figs. 5–7), hence assumption (i) does not hold. Further, in the Cu-Au alloy system, three-body terms $(k = 3)$ play an important role in producing the observed[3-7] asymmetry of the phase diagram about $x = \frac{1}{2}$ so that assumption (ii) is false. Furthermore, actual calculations (e.g., Fig. 8) show that, though the first-neighbor pair interaction is stronger, it is not *much* larger than the other interactions, so assumption (iii) is often not met either. Finally, when dealing with volume (or concentration) dependent interactions, the sum rules of Eq. (6.5) do not hold. Hence, a practical study of the ground state must deal with a larger number of parameters than the two ratios considered by Kanamori and Kakehashi. In addition, one is frequently interested not just in ground-state structures but also in configurations that have slightly higher energies and could conceivably form metastable structures when kinetic circumstances permit this.

Although restricted, the Kanamori-Kakehashi study is very enlightening. For any ratios $v_{2,2}/v_{2,4}$ and $v_{2,3}/v_{2,4}$, they found that only 40 fcc configurations can be ground states. These periodic structure have different numbers of atoms in the unit cell. They found that, in general, ground-state structures have rather small unit cells: only 8 possible breaking points have unit cells with more than 12 atoms per cell (or 12 fcc sites). Moreover, configurations with large unit cells, though theoretically belonging to the GSL, might be very difficult to grow because they require a long-range correlation between atomic positions. For these two reasons it is practical to study the ground state restricting ourselves to those configurations with unit cells of limited sizes. In adopting this view we might miss some breaking points in the GSL, but hopefully not many.

Our calculation of the ground state then proceeds in two steps.

(1) We construct a file of all fcc-based and bcc-based configurations with unit cells smaller or equal to a certain maximum size ($M = 16$ sites). For each configuration we store the values of $\overline{\Pi}_F$ for the figures of Table II. We have described elsewhere[89] a systematic procedure to construct this file, without missing any configuration, and without repetitions.

(2) Once the file is constructed, finding the ground state for a given set of interactions $\{J_F\}$ is carried out by computing $\Delta E(\sigma, V)$ of Eq. (5.8) and comparing $\{\Delta E(\sigma, V); X(\sigma)\}$ with the values for the configurations α and β [using Eqs. (6.1) and (6.2)] that up to this point were found to be the breaking points of the GSL. If Eq. (6.2) is *not* satisfied by the pair α, β that satisfy Eq. (5.8), configuration σ is a new breaking point. In this case we rescan the previously determined breaking points α and β, examining whether any of them are now excluded from the GSL due to the introduction of σ. Note, therefore, that we combine a *homogeneous* ground-state search (i.e., finding the lowest energy configuration for a fixed composition) with a *heterogeneous* search (i.e., comparing ground states of different compositions, identifying thereby true "breaking points").

B. Predicted ground-state structures

Figure 9 depicts the ground-state lines for the alloy systems studied here. The symmetries established clearly from experiment are also found theoretically, even though we have purposely omitted from the basis set used to extract J_F some of the structures which are *known* to be ground states. Note that while high-temperature-
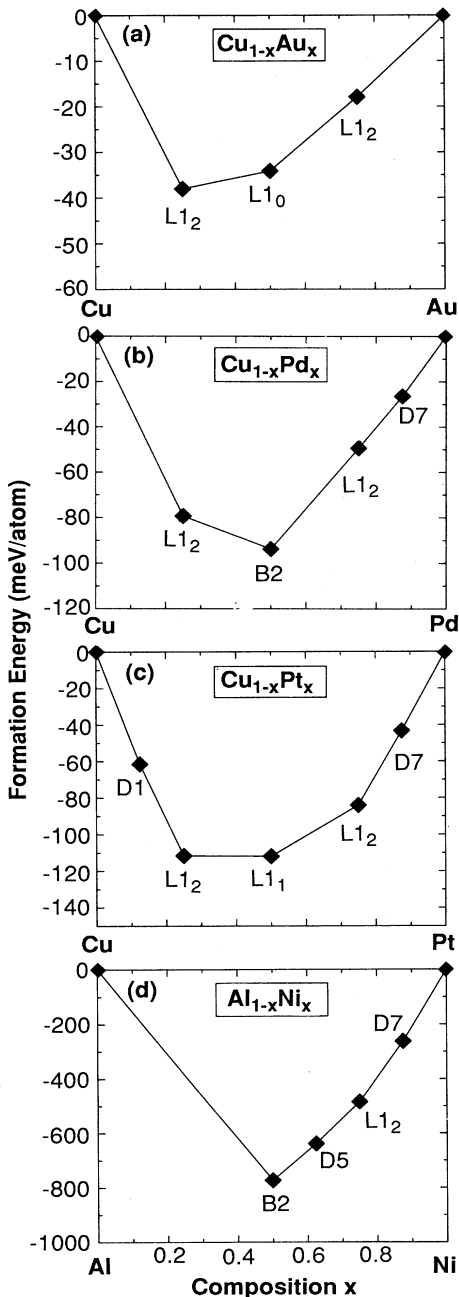

FIG. 9. Ground-state line for (a) $Cu_{1-x}Au_x$, (b) $Cu_{1-x}Pd_x$, (c) $Cu_{1-x}Pt_x$, (d) $Cu_{1-x}Rh_x$, and (e) $Al_{1-x}Ni_x$. Energies shown are for the unrelaxed cluster expansion [Eq. (5.8)].

ordered phases are relatively easy to detect experimentally, some of the potentially low temperature "ground-state structures" discussed in this section might be more difficult to observe (due to the slow atomic diffusion rates at low temperatures). In what follows we summarize the pertinent low temperature experimental data.

1. $Cu_{1-x}Pt_x$

Experimentally,[3-7] $Cu_{1-x}Pt_x$ [Fig. 1(c)] shows at low temperatures the fcc $L1_2$ structure of Cu_3Pt near $x=0.20$, and the rhombohedral $L1_1$ structure at $x=0.5$. At higher temperatures the $L1_1$ structure undergoes a first-order transition into the disordered fcc alloy at $812\,°C$. This transition is particularly interesting in that the number of unlike nearest neighbors is unchanged through the transition. At Pt concentrations above $x=0.5$ and low temperatures one finds a set of continuous transition into other ordered structures: the cubic $L1_2$ ($CuPt_3$), as well as the $CuPt_7$ and Cu_3Pt_5 structures. The crystal structures of the latter two phases are unknown, although both correspond to fcc modifications.

Our calculation is in substantial agreement with experiment. We find for CuPt the established Cu_3Pt ($L1_2$) and CuPt ($L1_1$) phases, i.e., we correctly describe the competition between rhombohedral ($L1_1$) and tetragonal ($L1_0$) symmetries. Two additional ground-state fcc compounds Cu_7Pt ("$D1$") and $CuPt_7$ ("$D7$"), having twice the primitive fcc lattice vectors are also identified; these were not included in the "basis set" as they were unsuspected by the normal method of guessing to be ground states (the $D1$ A_7B and $D7$ AB_7 structures are identical; they are depicted in Fig. 10). We tested our prediction by calculating the energy of Cu_7Pt ($D1$) directly from LAPW (finding $\Delta H=-65.5$ meV/atom), confirming the cluster expansion prediction ($\Delta H=-61.5$ meV/atom). Indeed an early[90] investigation did propose the existence of the $CuPt_7$ ("$D7$") structure on the basis of electric measurements (however, this was not directly confirmed by x-ray studies).

2. $Cu_{1-x}Pd_x$

Experimentally,[3-7] $Cu_{1-x}Pd_x$ [Fig. 1(b)] shows at low temperatures the bcc-type CsCl ($B2$) structure near $x=\frac{1}{2}$ and the fcc-type $L1_2$ structure around $x=0.19$. For $0.22\leq x \leq 0.25$ one finds a tetragonally deformed ($c/a \sim 0.986$) $L1_2$-like structure, best described as an antiphase boundary (APB) between adjacent $L1_2$ unit cells.[91,92] The ordered low temperature $L1_2$ phase undergoes a transition to this long-period superlattice structure (LPS) consisting of APB's at $470\,°C$ for $x=0.18$, and at $350\,°C$ at $x=0.21$. These long-period superlattice disorder above $\sim 500\,°C$ and may not exist at low temperatures.

Our calculated results [Fig. 9(b)] for CuPd show the observed fcc-type Cu_3Pd ($L1_2$) and bcc-type CuPd ($B2$) structures, indicating that our theory correctly reproduces the delicate balance between fcc and bcc interactions. The cluster expansion also predicts that $CuPd_3$ ($L1_2$) and $CuPd_7$ ($D7$) are only ~ 3 meV/atom
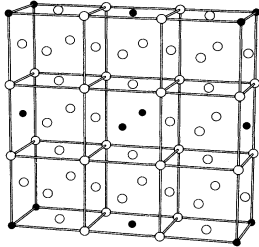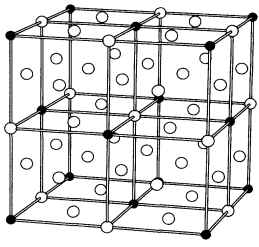
SB Name:	(Nb Ni$_8$)	(D1,D7)
Formula:	A$_8$B; AB$_8$	A$_7$B;AB$_7$
Crystal Structure ○A ●B		
Example:	NbNi$_8$	Ca$_7$Ge
Bravais Lattice:	Simple Tetragonal	Face - centered Cubic
Unit Cell Vectors	(0, 1/2, 3/2) (3/2, 0, 3/2) (3/2, 1/2, 0)	(0, 1, 1) (1, 0, 1) (1, 1, 0)
Space group: Pearson Symbol:	P4/mmm (D$^1_{4h}$)	Fm$\bar{3}$m (O^5_h) cF32
Superlattice:	None	None

FIG. 10. Crystal structure information for commonly occurring intermetallic transition metal alloys that are generally *not* observed in the CuAu and CuRh treated here. We use our cluster-expansion method to verify that these structures are indeed unstable (Sec. VI C). See caption to Fig. 3 for further details.

below the line connecting $B2$ $(x=\frac{1}{2})$ with Pd $(x=1)$, hence, could form at low temperatures.

3. $Cu_{1-x}Au_x$

Experimentally,[3-7] $Cu_{1-x}Au_x$ [Fig. 1(a)] shows at low temperatures the fcc-based Cu_3Au—I $(L1_2)$ cubic ordered structure at $x=\frac{1}{4}$. At $x=\frac{1}{2}$, $Cu_{1-x}Au_x$ forms the fcc-based Cu-Au-I $(L1_0)$ structure. This structure has a tetragonal distortion, with the c/a ratio between 0.931 to 0.938.[7(a)] At $T=658$ K, this Cu-Au-I phase transforms into the Cu-Au-II structure best described as one-dimensional LPS, with repeat period ~ 5 Cu-Au-I cells. This LPS disorders above ~ 683 K. The ordered structure seen for CuAu$_3$ at $x=\frac{3}{4}$, is, however, less certain: it is believed to be a two-phase mixture of the $L1_2$-type and a one-dimensional antiphase structure.[7(a)] Similarly, there exists a one-dimensional LPS denoted as the Cu$_3$Au-II phase. It occurs at Au-rich compositions with 18 Cu$_3$Au-I cells an antiphase domain boundary located after 9 unit cells.[7(a)]

Our calculation [Fig. 9(c)] for CuAu correctly identifies Cu$_3$Au $(L1_2)$, CuAu $(L1_0)$, and CuAu$_3$ $(L1_2)$ to be on the GSL. The Cu$_3$Au and CuAu structures are found to be very stable. On the other hand, the CuAu$_3$ is less stable: it moves above the GSL, when the structural relaxation is incorporated. This is consistent with the experimental fact that other structures can effectively compete with CuAu$_3$ at low temperatures.

4. $Cu_{1-x}Rh_x$

Experimentally,[3-7] $Cu_{1-x}Rh_x$ [Fig. 1(d)] exhibits fcc disordered solid solutions above 1150 °C. At lower temperatures, the phase field exhibits a wide miscibility gap corresponding to phase separation into Cu-rich and Rh-rich fcc alloys. Our calculation for CuRh shows indeed a trivial horizontal GSL (not shown in Fig. 9) representing phase separation, as observed.

5. $Al_{1-x}Ni_x$

Experimentally,[3-7] $Al_{1-x}Ni_x$ shows both fcc- and bcc-based structures. The presence of the CsCl $(B2)$ structure at $x=\frac{1}{2}$ and the $L1_2$ structure at $x=\frac{3}{4}$ is well established.[7(b)] In addition, a bcc-like Al$_3$Ni$_5$ structure has been identified recently at low temperatures at $x=\frac{5}{8}$.[7(b)] It is isotypical with Ga$_3$Pt$_5$ and shown in Fig. 11, where it is denoted as $D5$.

Our calculation are shown in Fig. 9(d). The presence of the cubic CsCl structure $(B2)$ and the NiAl$_3$ $(L1_2)$ phase in the ground state are correctly reproduced. These are very stable phases with properties studied by many authors.[3] At $x=\frac{5}{8}$ we find the $D5$ structure (Ga$_3$Pt$_5$-like) in the GSL. It is barely below the line joining the CsCl and $L1_2$ points in Fig. 9(d), which means that, if truly a stable phase, it exists only at lower temperatures. True Ga$_3$Pt$_5$ has an orthorhombic distortion which we have not considered, but which could lower its
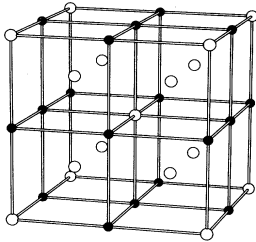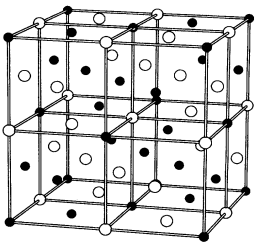
SB Name:	(D3,D5)	(D4)
Formula:	A_5B_3; A_3B_5	A_4B_4
Crystal Structure ○A ●B		
Example:	"Ga_3Pt_5"	
Bravais Lattice:	Body-centered Cubic	Face - centered Cubic
Unit Cell Vectors	(-1, 1, 1) (1, -1, 1) (1, 1, -1)	(0, 1, 1) (1, 0, 1) (1, 1, 0)
Space group: Pearson Symbol:	$Im\bar{3}m$, (O_h^9)	$Fd\bar{3}m$ (O_h^7)
Superlattice:	None	None

FIG. 11. Crystal structures, see caption to Fig. 10.

energy still further. At $x = \frac{7}{8}$ we predict the fcc-based configuration denoted $D7$ (see Fig. 10), whose stability is not an experimental fact.

In addition to these ground-state structures we have identified other metastable structures whose energies are not far from the GSL. For example, our calculations place the DO_{22} configuration just 2.2 meV above the ground state at $x = \frac{3}{4}$, while the DO_3 energy is further

SB Name:	(Mn_2Au_5)	($\gamma1,\gamma2$)
Formula:	$A_{10}B_4$; A_4B_{10}	A_2B;AB_2
Crystal Structure ○A ●B		
Example:	Mn_2Au_5	$MoPt_2$
Bravais Lattice:	Centered Monoclinic	Body- centered Orthorhombic
Unit Cell Vectors	(3/2, 0, -1/2) (1, 0, 2) (0, 1, 0)	(1/2, 1/2, 0) (0, 0, 1) (1, -1/2, 1/2)
Space group:	$C2/m$, (C_{2h}^3)	$Immm$ (D_{2h}^{25})
Pearson Symbol:	mC14	oI6
Superlattice:	$A_6B_2A_4B_2$ along [103]	A_2B along [110]
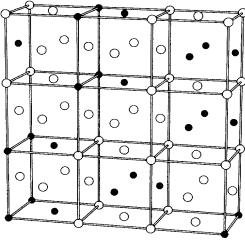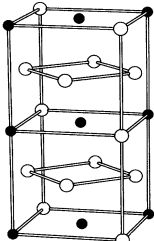
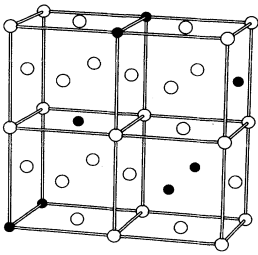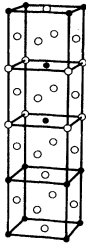FIG. 12. Crystal structures, see caption to Fig. 10.

	$D1_a$	DO_{23}
SB Name:	$D1_a$	DO_{23}
Formula:	A_4B; AB_4	A_6B_2;A_2B_6
Crystal Structure ○A ●B		
Example:	$MoNi_4$	$ZrAl_3$
Bravais Lattice:	Body-centered Tetragonal	Body - centered Tetragonal
Unit Cell Vectors	(3/2, 0, 1/2) (-1/2, 0, 3/2) (1/2, 1/2, 1)	(1, 0, 0) (0, 1, 0) (1/2, 1/2, 2)
Space group:	I4/m, (C_{4h}^5)	I4/mmm (D_{4h}^{17})
Pearson Symbol:	tI10	tI16
Superlattice:	A_4B along $[20\bar{1}]$	$A_5B_1A_1B_1$ along $[40\bar{1}]$

FIG. 13. Crystal structures, see caption to Fig. 10.

above.[88] At $x = \frac{3}{4}$ we find the DO_{23} structure, just 1.3 meV above the $L1_2$ structure: it can be characterized as an $Al_5Ni_1Al_1Ni_1$ superlattice along the [410] direction. It is hence an intermediate structure between the $L1_2$ and DO_{22} with ordering vector [201]. Finally, at $x = \frac{5}{6}$ we found a configuration just 0.9 meV above the GSL. It is a $Al_5Ni_3Al_1$ superlattice along the [531] direction.

Overall, we conclude that the local density functional description of structural energies correctly predicts the stable phases of these compounds (scanning $2^{16} = 65\,536$ structures for each compound), and identifies additional candidate low temperature phases.

C. Predicting formation energies of unstable structures

We have considered so far structures that are either ground states, or very nearly so; these are amenable to experimental observations. Since the cluster expansion is not limited to such structures, it might be interesting to consider trends in formation energies of *other* structures that are not observed for Cu intermetallics, but occur commonly in other intermetallics. Figures 10–13 describe such crystal structures, and Fig. 14 gives their predicted energies for $Cu_{1-x}Au_x$, $Cu_{1-x}Pd_x$, and $Cu_{1-x}Pt_x$. In all cases, they are above the ground-state line. We have performed LAPW calculations for some of the simplest structures in this group. The results (Table XVI) confirm the general trends in the predictions from the cluster expansion. We conclude that the latter can be used to reliably obtain energies of experimentally inaccessible structures. The trends in these energies observed in Fig. 14 are rather interesting: the DO_{23} structure is always a contender to the ground-state structures at $x = \frac{1}{4}$ and $x = \frac{3}{4}$, as is the $NbNi_8$-type structure at $x = \frac{1}{9}$ and $x = \frac{8}{9}$.

TABLE XVI. Comparison of the LAPW calculated formation enthalpies (meV/atom) of some common intermetallic structures (Figs. 10–13) *not* occurring in the CuAu, CuPd, and CuPt systems with predictions of the cluster expansion.

| | $Cu_{1-x}Au_x$ | | $Cu_{1-x}Pd_x$ | | $Cu_{1-x}Pt_x$ | |
Structure	LAPW	Clust.	LAPW	Clust.	LAPW	Clust.
A_4B_4 $(D4)$	66.8	71.5	−65.5	−61.0	−106.7	−82.0
A_2B $(\gamma 1)$	−10.4	−2.9	−73.3	−76.8	−84.2	−85.8
AB_2 $(\gamma 2)$	5.2	10.7	−41.6	−58.1	−29.9	−65.0
A_7B $(D1)$					−65.5	−61.5
AB_7 $(D7)$					−65.1	−43.6

D. The $L1_I$ and "$D4$" structures: an interesting observation

Figure 11 depicts the "$D4$" structure with composition A_4B_4: it has the fcc Bravais lattice and the $Fd3m$ space group. Inspection of its "lattice averaged spin products" $\overline{\Pi}_{k,m}(s)$ show that they are identical to those of the $L1_1$ structure of composition AB (having a trigonal Bravais lattice and space group $R\overline{3}m$; see Fig. 3) except for $J_{4,1}$ for which $D_{4,1}\overline{\Pi}_{4,1}(L1_1)=-2$ (Table III), while $D_{4,1}\overline{\Pi}_{4,1}(D4)=+2$ (this observation is due to F. Ducastelle, private communication, for which we ate grateful). Hence, all physical properties of these two structures which are *not* related to the four-body terms, should be identical. This suggests a simple method for calculating $J_{4,1}$ from

$$\Delta E(D4)-\Delta E(L1_1)=4J_{4,1} , \qquad (6.6)$$
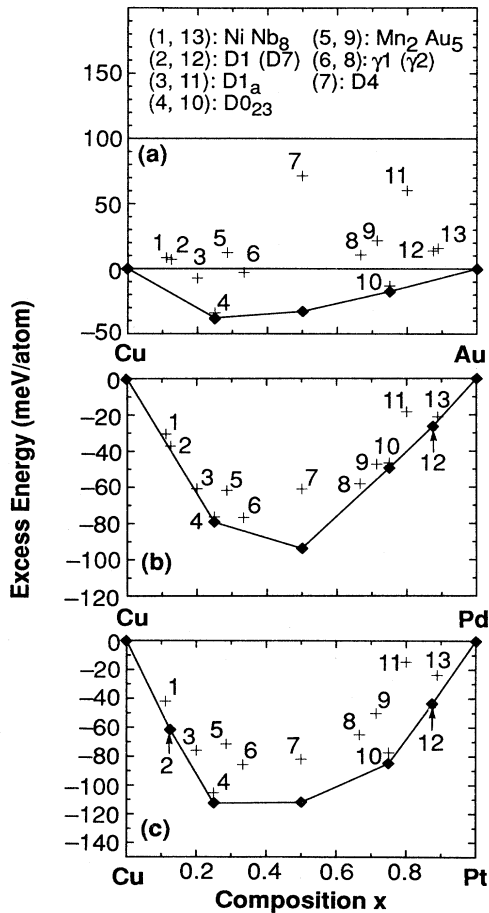
FIG. 14. The solid lines connecting diamond-shape symbols give the predicted ground-state structures; crosses gives the predicted (unrelaxed) energies of commonly occurring intermetallic compounds (Figs. 10–13) that are *not* stable for the alloys considered here. The symbols in the inset to part (a) refer to the structure types described in Figs. 10–13. (a) CuAu, (b) CuPd, and (c) CuPt.

independent of the cluster expansion. Unfortunately, $J_{4,1}$ is rather small for these systems (see Fig. 8), hence the uncertainty in these values is not negligible. Using, nevertheless Eq. (6.6), we find at $x=\frac{1}{2}$ that $J_{4,1}(CuPd)=0.3$ and $J_{4,1}(CuPt)=1.3$ meV compare with the values from the cluster expansion (Fig. 8) $J_{4,1}(CuPd)=1.5$ and $J_{4,1}(CuPt)=7.0$ meV, i.e., they are of the correct order of magnitude.

VII. FINITE-TEMPERATURE THERMODYNAMIC PROPERTIES

We have so far addressed the issue of $T=0$ "ground-state structures," finding some phases that are highly stable and well-documented experimentally (e.g., $L1_0$ in CuAu, $L1_1$ in CuPt, and $B2$ in CuPd), along with some phases whose energy is barely below the GSL (e.g., the $D5$ Al_3Ni_5 structure and the $D7$ AlN_7 structure); these correspond to structures that can disorder at low temperatures, hence might escape experimental detection. Although it is not our intention to discuss in this paper in detail the *finite-temperature* properties of these alloys, we will touch upon the issue of finite temperature stability for some of these structures, providing estimates for ordering temperatures. For example, in the case of Al-Ni, our calculated ground state presents the yet unreported phase $D7$. Although the ground-state calculation may be made following different procedures (different ways of handling the molar volume, e.g., by minimizing of the energy, or by expansion in a series of figures, see Sec. IV D) we always found that the $D7$ structure was present in the calculated ground-state line of Al-Ni. Another interesting feature of our Al-Ni results is that it clearly places the Ga_3Pt_5-like phase $D5$ also in the ground-state line. Earlier experimental determinations of the phase diagram[6] excluded this low temperature phase. Since the formation enthalpies of the Al-Ni ordered compounds are sufficiently large (Table XI) to make the LDA or cluster-truncation errors relatively unimportant, we were specially interested in using our first-principle interaction energies (Fig. 7) to calculate the resulting phase diagram by means of the cluster variation method (CVM).[93] It is well known that a phase diagram represents a delicate competition between phases of nearly equal energies. Hence even the topology of the phase diagram is highly sensitive to small errors in the energy parameters and constitutes a sensitive test of the LDA. It is not our intention to describe the details of the CVM; we just note that we have used the tetrahedron approximation[94] for calculations of *entropies*, while all $\{J_{k,m}\}$ interactions are included in the description of the *internal energies*. We used a correlation function program, and the Newton-Raphson method to find the solution of the nonlinear equations (not a density matrix program and the natural iterations[95]). The correlation functions for the pairs not contained in the tetrahedron, such as the figures $(k,m)=(2,2)$, $(2,3)$, $(2,4)$ for fcc, and $(2,3)$, $(2,5)$ for bcc, were expressed as products of the point correlation functions of their vertices.[96] This decoupling was very successful in the case of the calculation of the phases diagram of semiconductor alloys.[27(a)] Vibrational entropies and liquid-state effect were neglect-

ed in this calculation.

Figure 15(a) gives the observed[3,6] phase diagram; the calculated fcc and bcc solid phase portions of the $Al_{1-x}Ni_x$ phases diagram is given in Fig. 15(b). The lines of equilibrium are cut at $T = 1640$ K where melting begins.[97] The binodal of $B2$-$L1_2$ and $L1_2$-Ni equilibrium lines agree well with experiment at temperatures near melting.[7(b)]. At lower temperatures the $B2$-$L1_2$ binodal is deformed by the occurrence of the Al_3Ni_5 phase $D5$, which we find to be stable below 950 K. The experimental phase diagram near the onset of the $D5$ stability is not exactly reproduced by our calculation, but does not differ much from it. Thus, the onset of the $D5$ stability marks the appearance of a new parameter of order in the $B2$ medium. At lower temperatures, our $L1_2$-Ni binodal falls faster (vertically) than experiment, due to the presence of the stable $AlNi_7$ phase $(D7)$ in our calculations. This phase has never been reported, but the observed instability of the binodal[6] might be indicating the presence of a hidden phase like our $D7$. Since this phase has a very low Al concentration, and since its translation vectors are fcc-like (but doubled), this phase might be easily confused with fcc Ni with a random distribution of Al impurities.

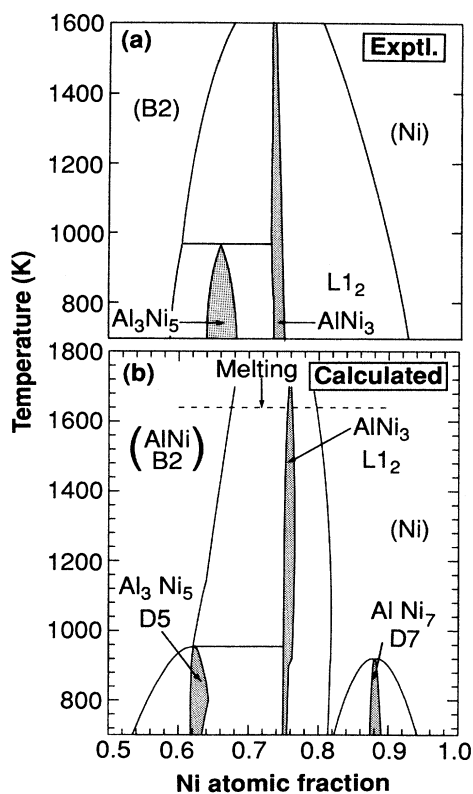The cluster variation method provides also the finite-temperature excess thermodynamic functions, such as the mixing enthalpies $\Delta H(x,T)$ and free energies $\Delta F(x,T)$ of, e.g., disordered (imperfectly random) alloys. We have noted in Sec. V D that the cluster expansion for *disordered* alloys converges well even using *relaxed* energies (Table XIV). We can hence use the *relaxed* interaction energies to describe $\Delta H(x,T)$. Figure 16 compares our CVM calculated thermodynamic properties with experimental data,[5] when available, showing reasonable agreement.

VIII. SUMMARY

We have shown that the informational content of total energy curves for $O(10)$ ordered A_nB_m structures suffices to determine a reasonably complete renormalized set of Ising-like interaction energies, and that this enables a "ground-state search" of $\sim 65\,000$ other structures. This removes much of the uncertainty underlying the use of the local density formalism to predict equilibrium struc-
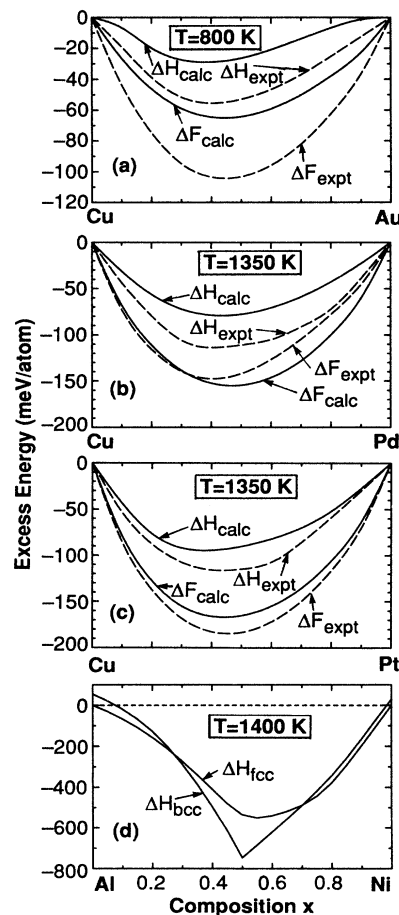

FIG. 15. (a) Experimental (Ref. 3) and (b) CVM calculations for the phase diagram of $Al_{1-x}Ni_x$ for $x \geq 0.5$. Vibrational entropy and liquid-state effects were neglected.

FIG. 16. Calculated CVM (using relaxed interaction parameter) and measured (Ref. 5) mixing enthalpies $\Delta H(x,T)$ and excess free energies $\Delta F(x,T)$ of the disordered phases of (a) CuAu, (b) CuPd, (c) CuPt, and (d) AlNi.

tures out of a limited set of only $O(10)$ possibilities. The most stable experimentally observed ground-state structures of $Cu_{1-x}Au_x$, $Cu_{1-x}Pd_x$, $Cu_{1-x}Pt_x$, $Cu_{1-x}Rh_x$, and $Al_{1-x}Ni_x$ are correctly identified and a few additional low-temperature candidate structures are offered as predictions. The same method for extracting renormalized interactions works for simpler lattice properties, such as molar volumes and electrostatic energies. A unified description of general atomic relaxations is, however, lacking. In addition to this shortcoming, the main approximations in our treatment are the following.

(i) Use of Vegard's rule for determining the equilibrium volumes. Section V B examined this approximation and found it to introduce negligible errors in all cases but $Al_{1-x}Ni_x$ for which this approximation was not used.

(ii) Neglect of vibrational entropies. This can contribute significantly when one contrasts different Bravais lattices (e.g., fcc versus bcc) at finite temperatures, a comparison avoided here.

(iii) Renormalization of the contribution of large figures to the entropy. This approximation was tested quantitatively against Monte Carlo simulations [Ref. 27(b) Fig. 15] and was found to introduce negligible errors in the enthalpy and phase diagrams.

(iv) Truncation of the cluster expansion and use of a finite number of structures to extract interaction energies. This is a rather controllable approximation whose consequences are checked quantitatively in our transferability tests (Tables XII–XVI).

[1] R. W. G. Wyckoff, *Crystal Structures* (Interscience, New York, 1963), Vol. 1.

[2] P. Villars and L. Calvert, *Pearson's Handbook of Crystallographic Data for Intermetallic Phases* (American Society for Metals, Metals Park, OH, 1985).

[3] *Binary Alloy Phase Diagrams*, edited by J. L. Murray, L. H. Bennett, and H. Barker (American Society for Metals, Metals Park, OH, 1986).

[4] W. G. Moffatt, *The Handbook of Binary Phase Diagrams* (Germium, Schenectady, NY, 1984).

[5] R. Hultgren, P. D. Desai, D. T. Hawkins, M. Gleiser, and K. K. Kelley, *Selected Values of the Thermodynamics Properties of Binary Alloys* (Amdrican Society for Metals, Metals Park, OH, 1973).

[6] P. M. Hansen, *Constitution of Binary Alloys* (McGraw-Hill, New York, 1958).

[7] (a) *Phase Diagrams of Binary Gold Alloys* edited by H. Okamoto and T. B. Massalski (ASM International, Materials Park, Ohio, 1987); (b) P. D. Desai, J. Phys. Chem. Ref. Data **16**, 109 (1987).

[8] L. Pauling, *The Nature of the Chemical Bond* (Cornell University Press, Ithaca, 1960).

[9] W. Hune-Rothery and G. V. Raynor, *The Structure of Metals and Alloys* (Institute of Metals, London, 1957).

[10] W. B. Pearson, *The Crystal Chemistry and Physics of Metal Alloys* (Wiley Interscience, New York, 1972); W. B. Pearson, *Development in the Structural Chemistry of Alloy Phases*, edited by B. C. Glessen (Plenum, New York, 1969).

[11] L. S. Darken and R. W. Gurry, *Physical Chemistry of Metals* (McGraw-Hill, New York, 1953); A. R. Miedema, J. Less-Common Met. **32**, 117 (1973); **46**, 67 (1976); A. R. Miedema, R. Boom, and F. R. DeBoer, *ibid.* **41**, 283 (1975).

[12] J. St. John and A. N. Bloch, Phys. Rev. Lett. **33**, 1095 (1974); A. Zunger, Phys. Rev. B **22**, 5839 (1980); J. R. Chelikowsky and J. C. Phillips, *ibid.* **17**, 2453 (1978).

[13] (a) O. Kubaschewski and C. B. Alcock, *Metallurgical Thermochemistry* (Pergamon, Oxford, 1979); (b) C. Kittel, *Introduction to Solid State Physics*, 5th ed. (Wiley, New York, 1976).

[14] C. Froese Fischer, *The Hartree-Fock Method for Atoms* (Wiley-Interscience, New York, 1977).

[15] See, e.g., E. M. Lifshitz and L. P. Pitaevskii, *Statistical Physics, Part 1* (Pergamon, New York, 1976).

[16] A recent review of results of total and structural energy calculations is given in (a) *Electronic Structure, Dynamics, and Quantum Structural Properties of Condensed Matter*, edited by J. T. Devreese and D. Van Camp (Plenum, New York, 1985); (b) *Alloy Phase Stability*, edited by G. M. Stocks and A. Gonis (Kluwer Academic, Dordrecht, 1989); (c) V. L. Moruzzi, J. F. Janak, and A. R. Williams, *Calculated Electronic Properties of Metals* (Pergamon, New York, 1978).

[17] C. Domb, in *Phase Transition and Critical Phenomena*, edited by C. Domb and H. S. Green (Academic, London, 1974), Vol. 3, p. 357.

[18] D. de Fontaine, in *Solid State Physics*, edited by H. Ehrenreich, F. Seitz, and D. Turnbull (Academic, New York, 1979), Vol. 34, p. 73.

[19] J. Kanamori and Y. Kakehashi, J. Phys. (Paris) Colloq. **38**, C7-275 (1977).

[20] A. Finel and F. Ducastelle, in *Phase Transformation in Solids*, edited by T. Tsakalakos, MRS Symposia Proceedings No. 21 (Materials Research Society, Pittsburgh, 1984), p. 293.

[21] T. Morita, Physica **133A**, 173 (1985).

[22] J. M. Sanchez, D. Gratias, and D. de Fontaine, Acta Crystallog. **38A**, 214 (1982).

[23] M. J. Richards and J. W. Cahn, Acta Metall. **19**, 1263 (1971); S. M. Allen and J. W. Cahn *ibid.* **20**, 423 (1972).

[24] A. G. Khachaturyan, Prog. Mat. Sci. **22**, 1 (1978).

[25] J. M. Sanchez, F. Ducastelle, and D. Gratias, Physica **128A**, 334 (1984).

[26] The internal energy of alloys can be calculated directly as a function of some restricted order parameters, e.g., see R. C. Kittler and L. M. Falicov, Phys. Rev. B **18**, 2506 (1978); R. J. Hawkins, M. O. Robbins, and J. M. Sanchez, *ibid.* **33**, 4782 (1986).

[27] (a) L.G. Ferreira, S.-H. Wei, and A. Zunger, Phys. Rev. B **40**, 3197 (1989); (b) S.-H. Wei, L. G. Ferreira, and A. Zunger, *ibid.* **41**, 8240 (1990); (c) a preliminary version of this work, using a different formulation of the interactions p_F is included in Z. W. Lu, S.-H. Wei, A. Zunger, and L. G. Ferreira, Solid State Commun. **78**, 583 (1991); (d) Z. W. Lu, S.-H. Wei, and A. Zunger (unpublished). The resulting ground-state structures differ slightly from what is found here (Fig. 9 below).

[28]I. M. Torrens, *Interatomic Potentials* (Academic, New York, 1972).

[29]C. R. A. Catlow and W. C. Mackrodt, *Computer Simulations in Solids* (Springer-Verlag, Berlin, 1982).

[30]A. I. Kitaigorodsky, *Mixed Crystals* (Springer-Verlag, Berlin, 1984).

[31]A. Warshal, in *Semiempirical Methods of Electronic Structure Calculations,* edited by G. A. Segal (Plenum, New York, 1977), Vol. 8, p. 133.

[32]M. P. Tosi, in *Solid State Physics,* Vol. 16, edited by F. Seitz, and D. Turnbull (Academic, New York, 1964). p. 1.

[33]V. Heine, in *Solid State Physics,* edited by H. Ehrenreich, F. Seitz, and D. Turnbull (Academic, New York, 1970), Vol. 24, p. 1; W. Harrison, *Pseudopotentials in the Theory of Metals* (Benjamin/Cummings, Menlo Park, CA, 1966).

[34]A. Zunger and E. Huler, J. Chem. Phys. **62**, 3010 (1975); E. Huler and A. Zunger, Phys. Rev. B **12**, 5878 (1975).

[35](a) P. N. Keating, Phys. Rev. **145**, 637 (1966); (b) R. Biswas and D. R. Hamann, Phys. Rev. Lett. **55**, 2002 (1985).

[36]R. Kikuchi, J. M. Sanchez, D. de Fontaine, and H. Yamaguchi, Acta Metall. **28**, 651 (1980).

[37]C. Sigli and J. M. Sanchez, Acta Metall. **33**, 1097 (1985).

[38]J. M. Sanchez, J. R. Barefoot, R. N. Jarrett, and J. K. Tien, Acta Metall. **32**, 1519 (1984).

[39]H. Popkie, H. Kistenmacher, and E. Clementi, J. Chem. Phys. **59**, 1325 (1973).

[40]P. Cenedese, A. Marty, and Y. Calvayrac, J. Phys. (Paris) **50**, 2193 (1989).

[41]S. M. Foiles, M. I. Baskes, and M. S. Dow, Phys. Rev. B **33**, 7983 (1986); M. S. Dow and M. I. Baskes, *ibid.* **29**, 2443 (1984).

[42]R. A. Johnson, Phys. Rev. B **39**, 12554 (1989); **41**, 9717 (1990).

[43]M. J. Stott and E. Zaremba, Phys. Rev. B **22**, 1564 (1980).

[44]J. K. Nørskov and N. D. Lang, Phys. Rev. B **21**, 2131 (1980).

[45]P. Lambin and J. P. Gaspard, J. Phys. F **10**, 651 (1980); **10**, 2413 (1980); A. Berera, H. Dreysse, L. T. Wille, and D. de Fontaine, *ibid.* **18**, L49 (1988); H. Dreysse, A. Berera, L. T. Wille, and D. de Fontaine, Phys. Rev. B **39**, 2442 (1989).

[46]A. G. Khachaturyan, *Theory of Structural Transformations in Solids* (Wiley, New York, 1983).

[47]B. L. Gyorffy and G. M. Stocks, Phys. Rev. Lett. **50**, 374 (1983).

[48]G. M. Stocks, D. M. Nicholson, F. J. Pinski, W. H. Butler, P. Sterne, W. M. Temmerman, B. L. Gyorffy, D. D. Johnson, A. Gonis, X-G. Zhang, and P. E. A. Turchi, in *High-Temperature Ordered Intermetallic Alloys II,* edited by C. C. Koch, C. T. Liu, N. S. Stoloff, and O. Izumi, MRS Symposia Proceedings No. 81 (Materials Research Society, Pittsburgh, 1987), p. 15.

[49]F. J. Pinski, D. M. Nicholson, G. M. Stocks, W. H. Butler, D. D. Johnson, and B. L. Gyorffy, *ICS88 3rd International Conference on Supercomputing,* Vol. 1, edited by L. P. Kartashev and S. I. Kartashev (Int. Supercomputing Inst., St. Petersburg, FL, 1988), p. 321.

[50]G. M. Stocks and H. Winter, in *The Electronic Structure of Complex Systems,* edited by P. Phariseau and W. M. Temmerman (Plenum, New York, 1984), p. 463.

[51]D. D. Johnson, D. M. Nicholson, F. J. Pinski, B. L. Gyorffy, and G. M. Stocks, Phys. Rev. Lett. **56**, 2088 (1986); Phys. Rev. B **41**, 9701 (1990).

[52]F. Ducastelle, and F. Gautier, J. Phys. F **6**, 2039 (1976).

[53]F. Ducastelle [Ref. 16(b)], p. 293.

[54]A. Bieber and F. Gautier, Acta Metall. **34**, 2291 (1986); **35**, 1839 (1987).

[55]A. Bieber, F. Gautier, G. Treglia, and F. Ducastelle, Solid State Commun. **39**, 149 (1981).

[56]M. Sluiter and P. E. A. Turchi, Phys. Rev. B **40**, 11215 (1989).

[57]C. Sigli and J. M. Sanchez, Acta Metall. **36**, 367 (1988).

[58]R. Alben, M. Blume, H. Krakauer, and L. Schwartz, Phys. Rev. B **12**, 4090 (1975); J. J. Rehr and R. Alben, *ibid.* **16**, 2400 (1977); R. Alben, M. Blume, and M. McKewon, *ibid.* **16**, 3829 (1977).

[59]L. C. Davis, Phys. Rev. B **28**, 6961 (1988); L. C. Davis and H. Holloway, Solid State Commun. **64**, 121 (1987).

[60]A. Gonis, W. H. Butler, and G. M. Stocks, Phys. Rev. Lett. **50**, 1482 (1983).

[61]J. W. D. Connolly and A. R. Williams, Phys. Rev. B **27**, 5169 (1983).

[62](a) K. Terakura, T. Oguchi, T. Mohri, and K. Watanabe, Phys. Rev. B **35**, 2169 (1987); (b) S. Takizawa and K. Terakura, *ibid.* **39**, 5792 (1989).

[63](a) J. M. Sanchez, Solid State Commun. **65**, 527 (1988); (b) A. E. Carlsson, Phys. Rev. B **40**, 912 (1989); (c) M. Sluiter, D. de Fontaine, X. Q. Guo, R. Podloucky, and A. J. Freeman, in *High-Temperature Ordered Intermetallic Alloys III,* edited by C. T. Liu, A. I. Taub, N. S. Stoloff, and C. C. Koch, MRS Symposia Proceedings No. 133 (Materials Research Society, Pittsburgh, 1989). (d) M. Sluiter, D. de Fontaine, X. Q. Guo, R. Podloucky, and A. J. Freeman, Phys. Rev. B **42**, 10 460 (1990).

[64]G. P. Srivastava, J. L. Martins, and A. Zunger, Phys. Rev. B **31**, 3561 (1985).

[65]A. Mbaye, L. G. Ferreira, and A. Zunger, Phys. Rev. Lett. **58**, 49 (1987).

[66](a) A. Mbaye, D. M. Wood, and A. Zunger, Phys. Rev. B **37**, 3008 (1988); (b) D. M. Wood and A. Zunger, Phys. Rev. Lett. **61**, 1501 (1988).

[67]L. G. Ferreira, A. Mbaye, and A. Zunger, Phys. Rev. B **35**, 6475 (1987); **37**, 10547 (1988).

[68]S.-H. Wei, A. Mbaye, L. G. Ferreira, and A. Zunger, Phys. Rev. B **36**, 4163 (1987); A. Zunger, S.-H. Wei, A. Mbaye, and L. G. Ferreira, Acta Metall. **36**, 2239 (1988). The formation enthalpies we calculated in that paper for the CuAu system differ slightly from those given here (Table X) due to better convergence in the Brillouin-zone sums in the present work.

[69](a) J. E. Bernard and A. Zunger, Phys. Rev. B**36**, 3199 (1987); **34**, 5992 (1986); (b) S.-H. Wei and A. Zunger, *ibid.* **39**, 3279 (1989); S.-H. Wei and A. Zunger, J. Vac. Sci. Technol. A**6**, 2597 (1988).

[70]M. F. Ling and D. J. Miller, Phys. Rev. **34**, 7388 (1986); **38**, 6113 (1988).

[71]D. J. Chadi, Phys. Rev. B **16**, 790 (1977).

[72]S.-H. Wei and A. Zunger, Phys. Rev. B **39**, 6279 (1989).

[73]A. Balzarotti, N. Motta, A. Czyzyk, A. Kisiel, M. Podgorny, and M. Zimnal-Starnawska, Phys. Rev. B **30**, 2295 (1984); A. Balzarotti, Physica **146B**, 150 (1987); A. Balzarotti, N. Motta, A. Kisiel, M. Zimnal-Starnawska, M. T. Czyzyk, and M. Podgorny, Phys. Rev. B **31**, 7526 (1985).

[74]P. Letardi, N. Motta, and A. Balzarotti, J. Phys. C **20**, 2583 (1987).

[75]M. Ichimura and A. Sasaki, J. Electron. Mater. **17**, 305 (1988); Phys. Rev. B **36**, 9694 (1987); J. Appl. Phys. **60**, 3850 (1986); Jpn. J. Appl. Phys. **26**, 246 (1987); **26**, 1296 (1987).

[76]J. L. Martins and A. Zunger, Phys. Rev. B **30**, 6217 (1984).

[77]In the case of bcc (Table II), one notices that we have omitted the fourth-neighbor pair (2,4) [with sites at (0,0,0) and (3,1,1)]

but included the fifth pair (2,5). This is so since passing from the origin to (3,1,1), following a path through nearest neighbors, one passes through the intermediate sites (1,1,1) and (2,0,0), while in going from the origin to the fifth neighbor at (2,2,2) only the intermediate site (1,1,1) is passed. This criterion is being used to establish an hierarchy of interactions permitting to select the most important figure prototypes. It must be checked in specific cases, if this hierarchy bears a relation to the way the series of Eq. (4.1) converges.

[78]O. K. Andersen, Phys. Rev. B **12**, 3060 (1975).

[79](a) P. P. Ewald, Ann. Phys. (Leipzig) **64**, 253 (1921). See also E. Madelung, Phys. Z. **19**, 524 (1918); H. M. Evjen, Phys. Rev. **39**, 675 (1932). (b) R. Magri, S.-H. Wei, and A. Zunger, Phys. Rev. B **42**, 11 388 (1990). In that work we expanded E_M in six pair energies ($N_F = 7$, $N_S = 7$), so the results differ slightly from Eq. (4.15) here, where only five pair energies are used, and $N_S = 12$.

[80]P. Hohenberg and W. Kohn, Phys. Rev. **136**, B864 (1964); W. Kohn and L. J. Sham, Phys. Rev. **140**, A1133 (1965).

[81]S.-H. Wei and H. Krakauer, Phys. Rev. Lett. **55**, 1200 (1985), and references cited therein.

[82]E. Wigner, Phys. Rev. **46**, 1002 (1934).

[83](a) U. von Barth and L. Hedin, J. Phys. C **5**, 1629 (1972); (b) V. L. Moruzzi, J. F. Janak, and A. R. Williams, *Calculated Electronic Properties of Metals* (Pergamon, Oxford, 1978); (c) H. J. Monkhorst and J. D. Pack, Phys. Rev. B **13**, 5188 (1976).

[84]H. Skriver, *The LMTO Method* (Springer-Verlag, Berlin, 1984).

[85]F. D. Murnaghan, Proc. Natl. Acad. Sci. USA **30**, 244 (1944).

[86]J. W. Davenport, R. E. Watson, and M. Weinert, Phys. Rev. B **37**, 9985 (1988).

[87]D. Hackenbracht and J. Kübler, J. Phys. F **10**, 427 (1980); A. R. Williams, J. Kübler, and C. D. Gelatt, Jr., Phys. Rev. B**19**, 6094 (1979).

[88]J.-H. Xu, T. Oguchi, and A. J. Freeman, Phys. Rev. B **36**, 4186 (1987); J.-H. Xu, B.I. Min, A. J. Freeman, and T. Oguchi, *ibid.* **41**, 5010 (1990); B. I. Min, T. Oguchi, H. J. F. Jansen, and A. J. Freeman, J. Magn. Magn. Mater. **54-57**, 1041 (1986).

[89]A. Zunger, S.-H. Wei, and L. G. Ferreira, Int. J. Supercomp. Appl. **5**, 34 (1991).

[90]A. Schneider and U. Esch, Z. Elektrochem. **50**, 290 (1944).

[91]J. Kulik, D. Gratias, and D. de Fontaine, Phys. Rev. B **40**, 8607 (1989).

[92]B. Broddin, G. van Tendeloo, J. van Landuyt, and S. Amelinckx, Philos. Mag. B **57**, 31 (1988).

[93]R. Kikuchi, Phys. Rev. **81**, 988 (1951).

[94]H. Ackermann, G. Inden, and R. Kikuchi, Acta Metall. **37**, 1 (1989).

[95]R. Kikuchi, J. Chem. Phys. **60**, 1071 (1974).

[96]T. Morita, J.Phys. Soc. Jpn. **12**, 753 (1957).

[97]F. J. Bremer, M. Beyss, E. Karthaus, A. Hellwig, T. Schober, J.-M. Welter, and H. Wenzl, J. Crystal Growth **87**, 185 (1988).